LITHOSPHERIC MECHANICS AND DYNAMICS OF VENUS

ROGER J. PHILLIPS
Washington University

CATHERINE L. JOHNSON
Carnegie Institution of Washington

STEPHEN J. MACKWELL
Penn State University

PAUL MORGAN
Northern Arizona University

DAVID T. SANDWELL
Scripps Institution of Oceanography

and

MARIA T. ZUBER
Massachusetts Institute of Technology

Lithospheric mechanical and dynamical properties are constrained on Venus by both flexural modeling and convection modeling. Estimates of effective elastic thickness T_e on Venus are obtained by fitting flexural expressions to topographic profiles and by matching gravity/topography relationships, as a function of wavelength, to flexural models. T_e values from profile matching for coronae and other tectonic features lie in the general range of 10 to 40 km. Most estimates from gravity/topography modeling lie between 20 and 40 km. An earlier analysis for Atla Regio is updated with a degree 90 gravity model, and T_e is estimated to be about 25 km. In order to use T_e estimates to constrain lithospheric temperature gradients or heat flow, an understanding of lithospheric rheology is required. We update estimates of the steady state creep properties of diabase, and conclude that the crust of Venus could be nearly as strong as the mantle. Observed multiple scales of deformation in the absence of a weak lower crust may require new models of lithospheric behavior, including the possibilities of strain or velocity weakening. Both moment-matching methods and inelastic flexural modeling have been used to estimate surface heat flow $\hat{q}$. Moment-matching methods yield heat flow estimates for coronae and other flexural topography in the range 45 to 100 mW m^{-2}. High heat flow estimates at smaller coronae may reflect the thermal processes of coronae origin. Inelastic flexural modeling at Artemis Chasma gives $\hat{q}<12$ mW m^{-2}, and this may reflect thermally old lithosphere. For the three hotspots Atla, Bell, and Western Eistla Regiones, $\hat{q}$ lies in the range 36 to 65 mW m^{-2}. If

an estimated 0 to 10 mW m^{-2} of hotspot excess heat flow is subtracted, then the background flux is consistent with a planet that lies between the somewhat sluggish convective style predicted for the terrestrial planets in the absence of plate tectonics and a more Earth-like behavior. A plausible model is that there is a difference in heat flow between the two planets because Venus operates with less thermal efficiency than Earth due to a lack of significant subduction and to convective stratification.

I. INTRODUCTION

Building on a foundation of earlier missions, imaging and altimetry data from the Magellan mission (Saunders 1992), gravity data collected from Magellan's elliptical and circular orbits (chapter by Sjogren et al.), laboratory measurements of rock strength under Venusian conditions (Mackwell et al. 1995,1996), and improved numerical modeling all provide insight into the present and past mechanical and dynamical state of the Venusian lithosphere. Models for the mechanical state of the lithosphere are constrained by the following observables:

1. Gravity—both spherical harmonic models and inversion or forward modeling of line-of-sight (LOS) accelerations;
2. Topography—used alone or in conjunction with gravity to provide direct boundary conditions on interior mechanical/density models and used to constrain spatial instability modes of both extensional and compressional lithospheric deformation;
3. Images—mechanical models predict stress fields, which can be compared with normal faults and rifts, reverse faults and folds, and strike-slip faults observed (or inferred) in SAR images. Images also reveal dominant wavelengths of folding and faulting, which can be related to strength stratification of the lithosphere;
4. Rock strength—laboratory measurements of the ductile strength of rocks are essential to models of lithospheric mechanical response, particularly the time scales involved. Creep properties are used directly to determine thermomechanical properties from estimates of elastic lithospheric thickness;
5. Radiogenic heat production—as determined through geochemical measurements by landed spacecraft.

This chapter focuses on the ways in which elastic thickness can be estimated from topography and gravity data, the results of such analyses, and how such estimates can constrain the thermal structure of the Venusian lithosphere.

Consideration of the state of the lithosphere cannot be decoupled from the state of mantle convection beneath (chapter by Schubert et al.). Solomatov and his colleagues in a series of papers (Solomatov 1993,1995; Solomatov and Moresi 1996; Moresi and Solomatov 1995) argue that because of the temperature dependence of viscosity, most terrestrial planets should presently be in a state of "stagnant lid convection," wherein the thermal lithosphere is

quite thick (hundreds of km) and is essentially immobile except very near its bottom. A planet can avoid this seemingly boring fate by having a plate tectonic regime wherein the entire lithospheric column can be recycled because brittle faults extend through the strong part of the lithosphere. A key question is whether or not the interpretation of the mechanical and dynamical properties of the present Venusian lithosphere are consistent with a thick stagnant lid, a more Earth-like behavior, or something in between. This is at present a point of considerable controversy. Convection models with wildly disparate surface heat fluxes are able to match geoid and topography data at volcanic rises on Venus. Elastic thickness estimates provide constraints on surface heat flux, and can help resolve this controversy.

The purpose of this chapter, then, is to review what has been inferred about the mechanical and dynamical state of the Venusian lithosphere and to indicate where there are differences of opinion and to explain, if possible, why such differences exist. A basic theme is to use the results of elastic and inelastic modeling to estimate the thermal state of the planet. We commence with two sections on estimating effective elastic thickness of the Venusian lithosphere from topographic profiles and from gravity/topography relationships. A review and update of crustal rheology and lithospheric strength then sets the stage to use elastic thickness estimates to infer mechanical lithospheric thicknesses and temperature gradients. The corresponding heat fluxes are interpreted in the context of mantle convection models, and the issue of lithospheric state (thick vs thin) is summarized. We also discuss the implications of the surface evidence for significant nonelastic deformation, this in light of the recent experimental measurements that imply the crust has high ductile strength.

II. FLEXURAL MODELING OF TOPOGRAPHY

A. Introduction

Lithospheric flexure can result from static or dynamic processes and provides constraints on spatial and/or temporal variations in lithospheric thickness and strength. Lithospheric thickness may be determined solely from modeling topographic flexure or by combining gravity and topography data. In this section we discuss flexural modeling of Magellan altimetry data (Ford and Pettengill 1992); Sec. III will review inferences of lithospheric thickness on Venus using both gravity and topography data. Lithospheric flexure on Venus was first inferred from Venera 15 and 16 altimetry data over Freyja Montes (Solomon and Head 1990). Magellan altimetry has revealed additional sites of possible flexural signatures; these are associated with coronae (Sandwell and Schubert 1992*a*; Moore et al. 1992; Johnson and Sandwell 1994; Brown and Grimm 1996; see the chapter by Stofan et al. for a description of coronae), chasmata (McKenzie et al. 1992) and rifts (Evans et al. 1992).

On Earth, flexural topography is observed predominantly at seamounts and subduction zones. If the flexure has persisted on geologic time scales,

models involving the bending of a thin elastic or elastic-plastic plate may be appropriate and can provide an estimate of the effective elastic plate thickness. A purely elastic flexure model also assumes that the lithosphere can sustain infinite stresses; however, laboratory studies suggest that the strength of the upper lithosphere is limited by pressure-dependent brittle failure (Byerlee 1978) and the strength of the lower lithosphere is limited by temperature and strain-rate dependent ductile flow (Goetze and Evans 1979; Brace and Kohlstedt 1980). We are interested in that part of the lithosphere that can support stresses over geologic time scales, i.e., the thickness of the *mechanical lithosphere*. This is defined as the depth at which the lithosphere has little strength (less than tens of MPa, usually) for an assumed strain rate. The mechanical lithosphere is thicker than the elastic lithosphere, which is simply a convenient mathematical construct. Methods for using inferred elastic plate parameters and lithospheric rheological models to estimate mechanical thicknesses are discussed in Sec. V of this chapter.

Simple two-dimensional Cartesian elastic plate models (Solomon and Head 1990; Johnson and Sandwell 1994; Evans et al. 1992; Sandwell and Schubert 1992*a*; Brown and Grimm 1996) and two-dimensional axisymmetric models (Moore et al. 1992) have been used by several authors to model potential topographic flexural signatures on Venus. A full inelastic model has also been applied to the topography at Artemis Chasma (Brown and Grimm 1996; see Sec. V). Here we present a global synthesis of these results. The reader is referred elsewhere for details of the modeling techniques. Flexure of a viscous lithosphere is discussed, with reference to both a simple model developed for terrestrial flexure (DeBremaecker 1977), and viscous/viscoelastic relaxation mechanisms.

B. Data

Locations of Venusian features for which flexural modeling of topography has been attempted are shown in Fig. 1 (Ford and Pettengill 1992). Most of these features were studied as part of a global survey of lithospheric flexure using Magellan data (Johnson and Sandwell 1994) that incorporated a previous study of flexure at four large coronae (Sandwell and Schubert 1992*a*). Preliminary results from flexural analyses at rifts (Evans et al. 1992) and at small coronae (Moore et al. 1992) are also available. In most studies, altimetry orbit profiles across a given feature were modeled, either individually or as a combined data set. A few studies used topographic profiles extracted from the global gridded altimetry data (the GTDR; Ford and Pettengill 1992). Inferred flexural signatures exhibit a topographic low (generally referred to in flexure literature as a moat or trench) adjacent to a lower amplitude topographic high (see Fig. 2). In practice, however, topographic noise can mask low amplitude outer rises. Another complication is that faulting on the outer trench wall can lead to very rough topographic profiles, which are difficult to model. Magellan synthetic aperture radar (SAR) data is a useful secondary source of data in flexure modeling, as tectonic deformation observed in the radar images can be compared with model-predicted surface stresses.

C. Thin Elastic Plate Models

Thin plate models are based on the assumption that the plate thickness is small compared with the flexural wavelength. The general differential equation for plate flexure can be solved in either polar or Cartesian coordinates. Flexural features on Venus have been modeled using either two-dimensional Cartesian models in which the topography is assumed to be continuous along-strike, or two-dimensional axisymmetric models (ring or disk loads). In Cartesian coordinates the general differential equation for two-dimensional plate flexure (assuming no shear tractions on the base of the plate) is

$$\frac{\mathrm{d}^2 M(x)}{\mathrm{d}x^2} + \frac{\mathrm{d}}{\mathrm{d}x}\left[N(x)\frac{\mathrm{d}w(x)}{\mathrm{d}x}\right] + \Delta\rho g_0 w(x) = q(x) \quad . \tag{1}$$

In Eq. (1), $M(x)$ is the bending moment, $N(x)$ is the horizontal force per unit length (or "in-plane load"), $q(x)$ is the loading force, $\Delta\rho$ is the density contrast, g_0 is mean planetary gravitational acceleration, and $w(x)$ is the plate deflection. Equation (1) can be solved for either an inelastic rheology (moment-curvature relationship is nonlinear and a numerical solution is required; see Sec. V) or an elastic plate (linear moment-curvature relationship and analytical solutions possible). For the elastic case, the bending moment can be expressed in terms of the flexural rigidity, which in turn is a function of the elastic plate thickness T_e (see Sec. V).

In this section we focus on elastic plate solutions to Eq. (1). Most studies have assumed zero in-plane force, $N(x)$, and in fact it can be shown that $N(x)$ is in general poorly constrained in elastic plate models (Mueller and Phillips 1995). On Venus, where many features exhibiting potential flexural signatures are coronae, it is important to know whether an axisymmetric model is required or whether the planform geometry of the feature being modeled can be approximated by a two-dimensional Cartesian geometry. This has been discussed in some detail in Johnson and Sandwell (1994): numerical simulations show that a two-dimensional Cartesian model provides an accurate representation of the elastic plate thickness or equivalently the flexural parameter α (Turcotte and Schubert 1982; Eq. (2), Sandwell and Schubert 1992*a*) as long as the planform radius of the feature under study is several times the flexural parameter. However, the simulations show that even when the flexural parameter/elastic thickness is well determined using the Cartesian approximation, an axisymmetric model must be used to obtain a reliable estimate of the load/bending moment.

Details of modeling procedures vary from study to study. The more common approach is to minimize the rms misfit between the predicted elastic plate deflections and topographic profile(s) across a given feature. This provides an estimate of the elastic plate thickness, and allows the computation of surface

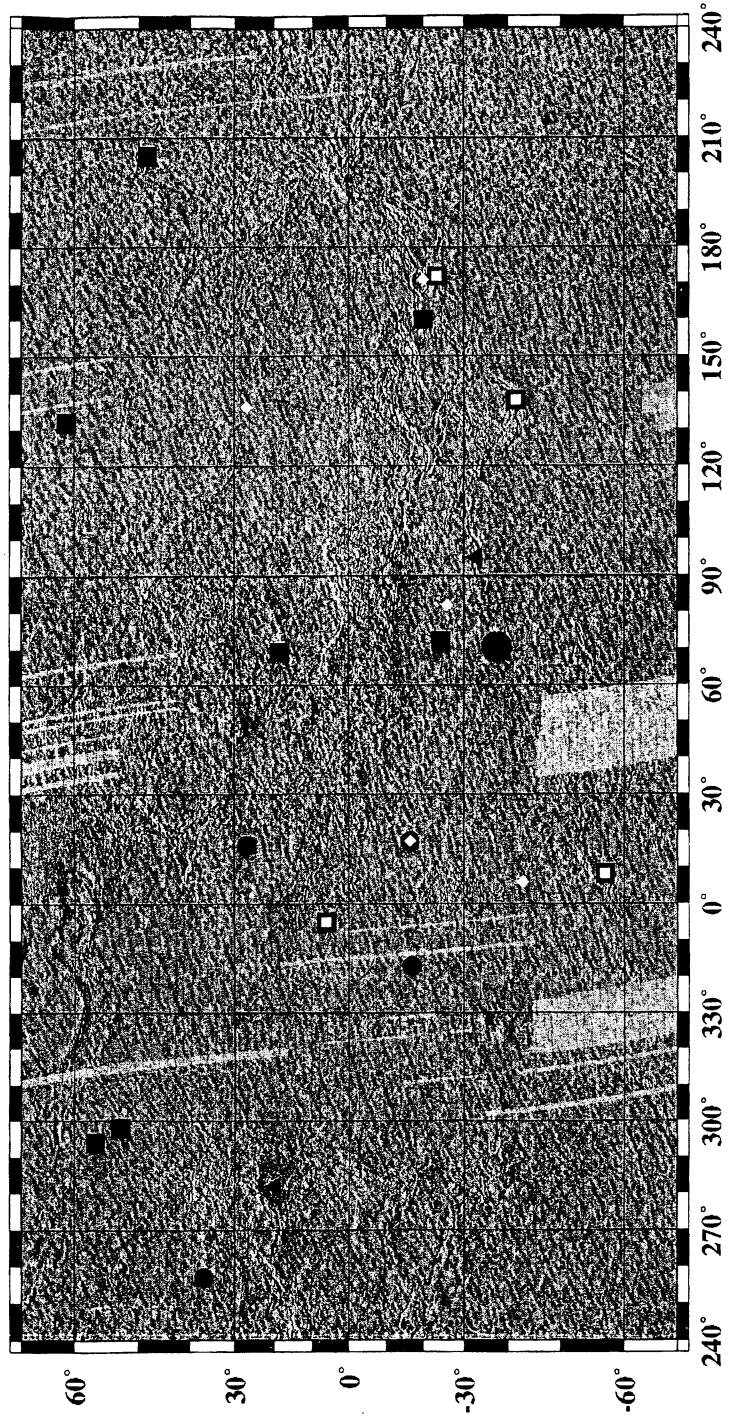

Figure 1. Mercator projection topography map of Venus illuminated from north (Ford and Pettengill 1992). Large black squares are features modeled using a two-dimensional Cartesian model and described in Johnson and Sandwell (1994); smaller white squares are features modeled using a two-dimensional Cartesian model and described in Sandwell and Schubert (1992*a*) (one area, Freyja Montes, is off the map at 78°N, 335°E). Black circles represent smaller coronae modeled in Johnson and Sandwell (1994), smaller white diamonds are coronae modeled with an axisymmetric model in Moore et al. (1992). Black triangles are rifts modeled using a two-dimensional Cartesian model and described in Evans et al. (1992).

stresses, bending moment and curvatures anywhere along a profile. An example of the application of this procedure to one corona on Venus (Nightingale corona) is shown in Fig. 2. The elastic plate thickness and plate curvatures can be used later, along with an assumed rheology, to estimate mechanical plate thickness and average lithospheric thermal gradients. In some cases only gross properties of the topographic profiles are modeled; e.g., the trench or outer-rise distance provides an estimate, albeit crude, of the elastic plate thickness in cases where modeling of the whole topographic profile is not possible (Johnson and Sandwell 1994). A summary of the results obtained from the application of elastic plate models to Venus is given in Table I. It can be seen that average or best-fit elastic thickness estimates fall in the range 5 to 56 km. Although elastic thickness does not provide direct information on lithospheric structure, it provides a lower bound on the mechanical lithospheric thickness and hence an upper bound on average thermal gradients. Estimates of mechanical thickness (or equivalently thermal gradients and heat flow) and implications for Venusian thermal and tectonic evolution are discussed in Secs. V and VII.

D. Flexure of a Viscous Plate

The elastic flexure model assumes that trench/outer rise features are statically maintained by large fibre stresses within a thin elastic lithosphere. Flexural features may also result from dynamical processes operating on a viscous lithosphere (DeBremaecker 1977; Melosh 1978). DeBremaecker (1977) derived a model for a hydrostatically supported viscous lithosphere, loaded at the trench and undergoing horizontal strain. The topography predicted by this model is indistinguishable from that predicted by an elastic plate model. In the viscous model, the parameter analogous to the flexural parameter of elastic plate models now incorporates both the horizontal strain rate and the thickness of the viscous lithosphere. Strain rate and viscous plate thickness are inversely proportional in these models. We have no evidence for large present-day strain rates on Venus (Grimm 1994); thus, as for elastic and inelastic flexure models, these viscous/viscoelastic plate models imply large viscous plate thicknesses and low thermal gradients. Another alternative is that the flexural signatures around, for example, coronae are the result of gravitational relaxation of topography produced earlier in the corona's evolution (Janes et al. 1992; Janes and Squyres 1995). New crustal rheologies for dry diabase (Mackwell et al. 1995,1996; also discussed in this chapter) suggest extremely long relaxation time scales, and hence it may not be surprising that we see so few coronae with associated flexural outer rise signatures (chapter by Stofan et al.). If gravitational relaxation is the mechanism whereby flexural signatures are produced, then the small number of observed flexural features at coronae suggest that most coronae on Venus are relatively young, consistent with evidence from impact crater densities, which imply that, on average, coronae are young relative to the mean surface age of the planet (Namiki and Solomon 1994; Price and Suppe 1994). We note, however, that

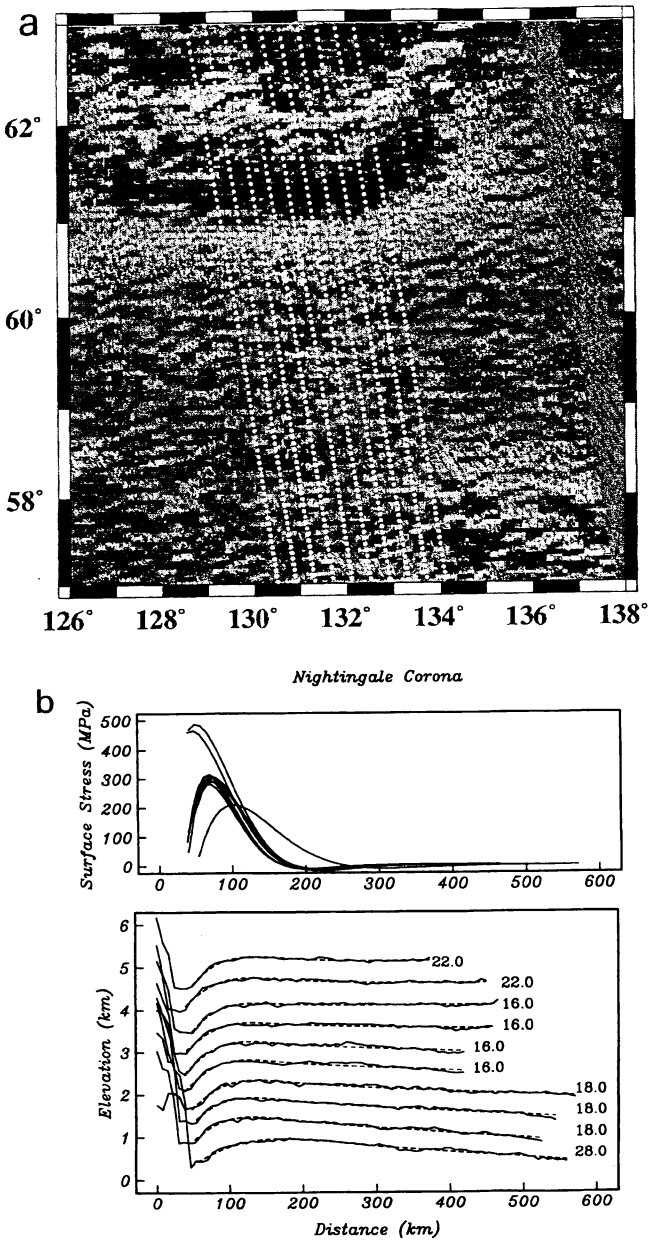

Figure 2. Results of Cartesian flexure modeling at Nightingale corona. (a) Shaded relief, with altimetry orbit tracks marked. (b) Lower plot shows altimetry orbits modeled (solid line), with the best-fit Cartesian elastic model (dashed line). Distance is calculated relative to the highest point of the topography inboard of the flexural moat. Elastic thickness corresponding to the best-fit model is given at the end of each profile. The upper figure shows the surface stresses predicted by the best fit models. The three anomalous surface stress profiles correspond to the upper 2 and lowermost altimetry profiles in the lower figure (those fit by a thicker plate) (figure from Johnson and Sandwell 1994).

TABLE I

Elastic Thickness Estimates from Topographic Profiles

Feature Name	Location		T_e (km)		Reference
	lat (°)	lon (°)	best/ave	Range	
Nishtigri Corona	−24.5	72.0	12	10–16	JS[a]
Neyterkob Corona	48.5	205.0	14	12–18	JS
Ridge	18.6	69.0	18	14–22	JS
Nightingale Corona	61.0	131.0	22	16–30	JS
S. Demeter Corona	53.0	298.0	22	16–32	JS
N. Demeter Corona	57.0	294.0	24	18–28	JS
W. Dali Chasma	−20.0	160.0	34	26–40	JS
Artemis Corona	−41.5	138.0	37	30–45	SS[b]
//			56		BG[c]
Latona Corona	−23.5	172.0	35	30–45	SS
//	−20.0	171.0	30		Me[d]
Eithinoha Corona	−57.3	8.2	18	12–24	SS
Heng-O	6.0	355.0	38	35–40	SS
Freyja Montes	78.0	335.0	16	15–25	SS
//				11–18	SH[e]
Indrani Corona	−37.5	70.5		4–7	JS
Bhumidevi Corona	−17.0	343.0		16–29	JS
Unnamed Corona	37.0	257.0		8–15	JS
Beyla Corona	27.0	16.0		8–13	JS
Fatua Corona	−16.5	17.2		5–10	JS
//	−17.0	17.0	15		Me
Selu Corona	−43.0	6.0	10		Me
Aramaiti	−26.0	82.0	10		Me
Boann	27.0	136.0	5		Me
Juno Dorsum	−33.0	92.0		8–20	Ee[f]

[a] JS = Johnson and Sandwell (1994); [b]SS = Sandwell and Schubert (1992*a*); [c]BG = Brown and Grimm (1996); [d]Me = Moore et al. (1992); [e]SH = Solomon and Head (1990); [f]Ee = Evans et al. (1992).

the theoretical relaxation profiles of coronae, while exhibiting a moat, display only very subtle outer rise flexural bulges, which occur late in their evolution (Janes and Squyres 1995).

III. FLEXURAL MODELING USING GRAVITY DATA

A. Introduction

In addition to flexural modeling using topographic profiles alone, flexural studies have been carried out using relationships between gravity and topography, as a function of wavelength. This "transfer function" approach is well established for the Earth with both isostatic and flexural studies (Dorman and Lewis 1970; Lewis and Dorman 1970; McKenzie and Bowin 1976; Forsyth

1985; McNutt and Shure 1986; Bechtel et al. 1987; McNutt 1988; Ebinger et al. 1989; Zuber et al. 1989). Difficulties in transferring the technique to Venus arise because the short wavelengths that are often necessary to infer lithospheric properties are not uniformly resolved in the gravity data.

Phillips (1994), Smrekar (1994), Smrekar et al. (see their chapter), and McKenzie and Nimmo (1996) have all determined lithospheric parameters using models matched to estimates of the admittance and/or coherence spectra. Most of these analyses were carried out at large volcanic rises, interpreted to be hotspots (see the chapter by Smrekar et al.). One straightforward and useful model involves an effective elastic thickness T_e (or flexural rigidity D), a crustal thickness z_m, a depth to bottom or subsurface load z_l, and the ratio f of the weight of a subsurface load to the weight of a surface load (Forsyth 1985). The physical basis of the model is in the Fourier transform of the three-dimensional version of Eq. (1). The model can be generalized for multiple density interfaces and multiple subsurface loads.

B. Modeling Ambiguity

In the absence of specific knowledge, we might assume only two dominant density contrasts within the Venusian lithosphere—at the surface and at the crust-mantle boundary. On Venus, one might anticipate a lithosphere loaded from above by volcanic constructs, for example, and from below by the buoyancy associated with thermal thinning of the lithosphere and with convection in the mantle. Clearly, the challenge is to account for all of these effects, and assumptions are usually required to make any progress. One approach is to assume that different processes operate in different portions of the wavelength spectrum. This is the basis of the approach of McNutt (1988), who applied the linear filters of McNutt and Shure (1986) to isolate longer wavelength hotspot swells (representing loading from below) from volcanic top loading at shorter wavelengths.

But Moresi and Parsons (1995) demonstrated with temperature-dependent viscosity convection calculations that coupling between long-wavelength temperatures and short wavelengths in the viscosity field produces a flat free-air admittance spectrum at short wavelengths, which is characteristic of uncompensated topography. Inversion of a short wavelength admittance spectrum for the flexural properties of the lithosphere might tend to overestimate elastic thickness if the spectrum is attributed solely to a finite flexural rigidity. However, the flat admittance spectrum of uncompensated topography is quite different than the sloped spectrum of flexurally compensated topography, so *a priori* there would seem to be little chance for confusion if one or the other process dominates. Unfortunately, not all convection models predict a flat spectrum (see, e.g., Fig. 11c in the chapter by Smrekar et al.), so a general statement about the ability to use spectral shape to separate convection effects from flexural effects is not possible at this time.

It has been suggested that spectral methods that assume that the top and bottom loads are statistically independent (see, e.g., Forsyth 1985) will resolve the two contributions (short wavelength convective effects, finite flexural rigidity) to the behavior of the gravity and topography fields (Moresi and Parsons 1995). Additionally, it is reasonable to subdivide the spectrum in such an analysis, as the ratio of bottom to top loading f is not expected to be constant across the spectrum (McNutt and Shure 1986; Phillips 1994), and in general we should consider that f is a function of wavenumber k.

C. A Synthetic Inversion

The idea that a Forsyth-type model can separate convective loading from surface loading can be tested by inverting synthetic admittance spectra. Using a four-parameter flexural model (Forsyth 1985), we inverted a synthetic admittance spectrum generated by Kiefer (1995) from a plume convection model with a Rayleigh number of 10^7 and a 65-km-thick high viscosity lid (see Fig. 11c in the chapter by Smrekar et al.). Even without temperature-dependent viscosity, such convection models produce significant spectral energy over the wavelength band one might use for flexural studies (~1000 km down to the 420 km cutoff of a deg 90 gravity model [chapter by Sjogren et al.]) (see Fig. 11a,b in the chapter by Smrekar et al.). Clearly, this renders suspect flexural rigidity (and elastic lithospheric thickness) estimates derived from gravity data, particularly over volcanic rises, whose most likely origin is still thought to be mantle plumes (Phillips and Malin 1983). The same holds true, of course, for flexural estimates in terrestrial hotspot regions (see, e.g., McNutt 1988; Ebinger et al. 1989).

However, the inversion of the synthetic admittance spectrum yielded a ratio of bottom to top loading f of infinity, which is exactly consistent with the convection model used to generate the gravity and topography "data." Secondly, the depth to bottom loading z_l found (225–250 km) is consistent with the thermal boundary layer of the plume model. The elastic thickness of 90 km obtained from the inversion may or may not be a surrogate for the high viscosity lid. Until complex models involving both temperature-dependent convective loading and flexural loading are examined, perhaps nothing can be said confidently about lithospheric properties derived from Venusian gravity data. However, it is equally clear that some insight can be obtained from the inversion itself, particularly if methods such as that of Forsyth (1985) can really separate convective bottom loading from flexural top loading (Moresi and Parsons 1995), and from examining the geologic setting of the region in question. First, it is necessary to establish with reasonable certainty the statistical independence of top and bottom loading, which is an inherent assumption of the approach. If a short-wavelength inversion yields a bottom loading depth of a few hundred kilometers or more and a large value of f, then one ought to suspect a significant component of convective loading and extreme caution should be used in elastic thickness interpretations. Conversely, if both z_l and f are small, then it may be reasonable to conclude that convective loading is unimportant. If in this case the terrain being studied is dominated at short wavelengths by gravity anomalies associated

with specific features (such as shield volcanoes) that appear to be loading the surface, then the argument is strengthened, albeit in a qualitative way. However, the most general case at hotspots on Venus may be a mixture of top and bottom loading.

D. Atla Regio Revisited with a Degree 90 Gravity Model

With these caveats in mind, we revisited the estimate for effective elastic thickness obtained by Phillips (1994) for the Atla Regio area—an analysis of a ~3500×3500 km region based on gravity data from a spherical harmonic model of degree $\ell = 60$ (Konopliv and Sjogren 1994). In 1993, the Magellan spacecraft was placed in a near circular orbit and higher degree spherical harmonic gravity solutions became possible. An $\ell = 90$ solution was available when this was written (MGNP90LSAAP; see the chapter by Sjogren et al.). Although tracking of the near-circular orbit did not take place over the Atla region, the inherent resolution in the tracking data from previous elliptical-orbit tracking exceeds that of $\ell = 60$ models at Atla.

Phillips (1994) argued that the loading ratio $f(k)$ at Atla Regio could be approximated as a piecewise constant function in two spectral bands with a common boundary at a wavelength λ of approximately 1000 km. Figure 3 plots admittance estimates for deg 60 and deg 90 gravity models, along with the mean Monte Carlo lithospheric model from Phillips (1994), in the short wavelength band. Good spectral estimates are possible down to λ = ~700 km and ~500 km for $\ell = 60$ and 90, respectively. Using the same annuli spacing for wavenumber averaging, the first three spectral estimates of $\ell = 90$ (circles) are close to $\ell = 60$ (diamonds). However, there is a significant scatter in the $\ell = 90$ estimates, which can be smoothed considerably by increasing the averaging interval slightly (squares). The smaller slope of this smoothed estimate presages an elastic thickness smaller than the 45-km value found by Phillips (1994).

Figure 4 shows an application of the model-fitting techniques of Phillips (1994) to the smoothed $\ell = 90$ admittance and Bouguer coherence spectra. The solid curves indicate the result of Monte Carlo modeling simultaneously of the admittance and coherence, while the medium- and short-dashed lines are the results, respectively, of Marquardt inversions (Press et al. 1992) of the admittance and coherence separately. There were no Monte Carlo results that produced solutions within the estimated errors. Allowing solutions to fit to within 6% produced 74 solutions in 10^7 runs. Note that only slightly different coherence curves produce significantly different elastic thickness estimates (10 km, Monte Carlo; 17 km, Marquardt), indicating that shorter wavelengths, where coherence spectra should have steeper slopes, are required to resolve the elastic thickness with a coherence model. This suggests that fitting the admittance only might be more useful, and a Marquardt inversion yields an elastic thickness of 27 km and is a better fit than the Monte Carlo result obtained jointly on admittance and coherence. For the Marquardt inversion on admittance, the crustal thickness z_m was set to 25 km and the solution

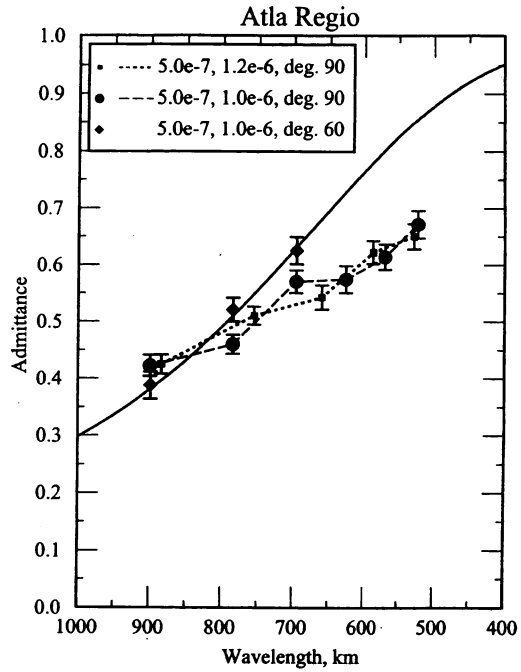

Figure 3. Dimensionless admittance spectrum in short wavelength band defined in Phillips (1994). Three spectral estimates are obtained in the $\ell = 60$ gravity model, and five in the $\ell = 90$ model. The first column in the legend refers to the wavenumber (m^{-1}) of the radius of the first annulus in the spectral averaging and the second column refers to the subsequent annuli spacing increment. The solid line shows the admittance of the mean Monte Carlo model from Phillips (1994): $f = 0.10$, z_m = 30 km, z_l = 7 km, and T_e = 45 km.

set is $f = 0.18$, z_l = 107 km, and T_e = 27 km. Setting z_m to 10 km yields $f = 0.19$, z_l = 112 km, and T_e = 30 km. (A slightly more conservative philosophy excludes the shortest-wavelength admittance estimate because at wavelengths shortward of ~600 km there is a sharp increase in the phase of the gravity/topography cross spectrum and a sharp decrease in the power in the two individual spectra. However, a new inversion (z_m = 25 km) increases T_e by only 2 km.)

To gain insight into parameter ranges and correlations, we carried out 10^8 Monte Carlo runs on admittance only; 3220 solutions were produced that generated model admittance values within the estimated errors. The search ranges were 0 to 1, 0 to 50 km, 0 to 400 km, and 0 to 50 km, respectively, for f, z_m, z_l, and T_e. A crustal thickness of 50 km is a sensible upper bound (see the chapter by Grimm and Hess). The solution properties are $f = 0.17 \pm 0.08$, z_m = 38±9 km, z_l = 131±57 km, and T_e = 25±3 km. The errors are the

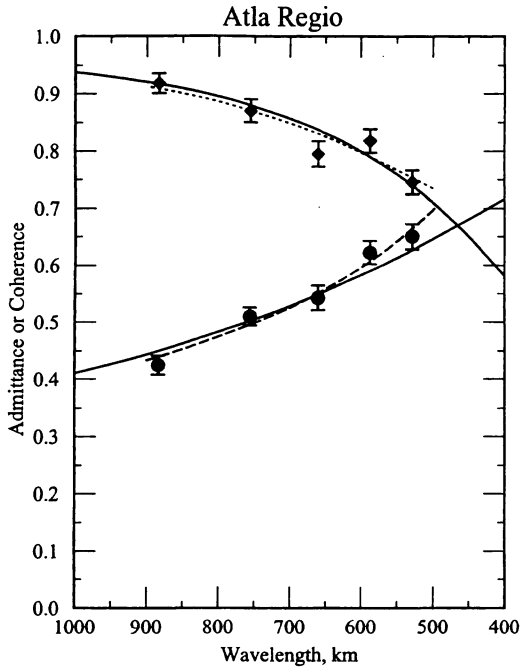

Figure 4. Results of Forsyth (1985) model fitting to smoothed $\ell = 90$ dimensionless free-air admittance (circles) and Bouguer coherence (diamonds) spectra. Solid curves are the results of Monte Carlo modeling, allowing solutions that matched all admittance and coherence estimates within 6%; in 10^7 runs, 74 solutions were obtained. The best fit is shown; it has solution parameters $f = 0.35$, $z_m = 4$ km, $z_l = 88$ km, and $T_e = 10$ km. The short-dashed line is the result of a Marquardt inversion on the Bouguer coherence and has solution parameters: $f = 0.37$, $z_m = 5$ km, $z_l = 95$ km, and $T_e = 17$ km. This suggests that in the Monte Carlo solutions, the first three parameters are controlled predominantly by the coherence. The medium-dashed line is the result of a Marquardt inversion on the admittance with z_m set to 25 km and has solution parameters: $f = 0.15$, $z_l = 108$ km, and $T_e = 27$ km.

estimated parameter standard deviations of the 3220 solutions. Parameter correlations were examined in solution scatter plots. Elastic thickness, T_e, was well bounded and poorly correlated with load depth z_l. There was also a poor correlation of z_l to loading ratio f. The results did indicate that top-loading dominates in this wavelength band, but either $f \approx 0.1$, and z_l is not well constrained, or $z_l \approx 80$ km, and f lies between 0.1 and 0.5. Crustal thickness was poorly constrained in these solutions and showed a strong negative correlation with the lower bound on elastic thickness. However, there was a minimum in elastic thickness at $z_m = 80$ km, and if the crustal search range was extended to an implausible upper limit of 100 km, then $T_e = 19 \pm 4$ km (and 24 ± 6 km for an absurd upper limit of 400 km).

E. Summary

A tabulation of elastic thickness estimates by gravity methods for different regions of Venus is given in Table II. Results depending on either the degree 90 spherical harmonic gravity model or LOS gravity data to extend spatial resolution to better than ~600 to 700 km seem to settle on a value for the elastic thickness at Atla Regio of 30 ± 5 km. It is important to note that the Atla estimates have been obtained by distinct methods of data analysis: (*i*) localization of the spherical harmonic fields to the Atla area followed by a Cartesian spectral analysis (Phillips 1994); (*ii*) localized inversion of LOS gravity data to a surface density representation followed also by a Cartesian spectral analysis of the corresponding gravity field (Smrekar 1994; Phillips 1994); and (*iii*) Fourier transforms of localized LOS gravity data to estimate directly the admittance (McKenzie and Nimmo 1996).

All of the results in Table II are based on spectral methods; they use relationships between gravity (or geoid) and topography as a function of wavelength, in conjunction with simple models, to estimate elastic thickness. Phillips (1994) and the new results for Atla given above use a combination of coherence and admittance estimates to invert for model parameters. McKenzie and Nimmo (1996) differentiated LOS Doppler velocity residuals to obtain an estimate of LOS gravity that contained higher spatial resolution than the traditional version of this product, where the use of cubic splines can result in oversmoothing. They used a top-loading flexural model ($f \equiv 0$) to obtain estimates of z_m, T_e, and ρ_c over that part of the wavelength spectrum they argue is dominated by flexure.

Smrekar (1994) and Smrekar et al. (see their chapter) also used admittance and coherence estimates to estimate elastic thickness. In addition, they used the linear filter approach of McNutt and Shure (1986) to separate bottom-loading from top-loading effects. This technique represents a means of specifying the spectral dependence of the loading ratio f. Finally, we note that Simons (1996) used a spatio-spectral localization technique directly on the spherical harmonic models to examine local admittances. The advantages of this technique are that it works directly with the spherical harmonic fields to localize the fields and quantify the spectral behavior (e.g., shortest resolvable wavelength) in any given region. The latter step is accomplished in Cartesian spectral analysis using information from the power, phase, and coherence spectra. In Simons (1996, Fig. 3.17), the admittance spectra at Bell and Atla Regiones are relatively flat over most of the spherical harmonic spectrum but have a sharp upturn at about 900 to 1000 km wavelength. The flat long-wavelength spectra are consistent with certain classes of convection models and the upturn can be interpreted in terms of flexure. This same behavior is seen, for example, in Cartesian spectra (Phillips 1994, Fig. 4; Smrekar 1994, Figs. 10 and 11). Simons employs a top-loading flexural model, and his results (Fig. 3.17) for Bell and Atla are consistent with the information given in Table II.

TABLE II
Elastic Thickness Estimates from Gravity-Topography Spectral Analyses

Region	Location		T_e (km)		Reference
	Lat (°)	Lon (°)	Best/Avg.	Range	
Atla Regio	−10 to 25	180 to 215	45	37–52	RP[a]
			25	22–28	TC[b]
			30	20–40	SS[c]
			35		MN[d]
Bell Regio	20 to 40	40 to 60		25–35*	SS
				45–55$^+$	
			15*		SK[e]
			40$^+$		
Beta Regio	16 to 39	272 to 295	30		MN
W. Eistla Regio	10 to 33	343 to 10		30–50	SS
			30		MN
			25*		SK
			45$^+$		
Ovda Regio	−15 to 7	70 to 110	$\lesssim$20		MN
Ishtar Terra	55 to 80	305 to 80	$\lesssim$15		MN
Alpha Regio	−35 to −18	355 to 10		~25–30	MN

[a] RP = Phillips (1994); [b]TC = this chapter; [c]SS = Smrekar (1994); [d]MN = McKenzie and Nimmo (1996); [e]SK = chapter by Smrekar et al.; * = short-wavelength result; $^+$ = long-wavelength result.

IV. RHEOLOGY AND LITHOSPHERIC STRENGTH

A. Introduction

An understanding of the tectonic behavior of the lithosphere and underlying mantle on Venus requires knowledge of the mechanical properties of the materials that comprise the Venusian crust and mantle. The elastic thickness of a lithosphere, as described in the previous two sections, is a surrogate for the complex rheology that comprises the real mechanical lithosphere. This does not diminish the importance of obtaining elastic thickness estimates, for it is a relatively straightforward parameter to obtain using topography and gravity data. In turn, one can often estimate the equivalent mechanical lithospheric thickness, or, more precisely, an equivalent inelastic bending moment. However, to make any use of this equivalent bending moment, or to solve the problem directly for loading of an inelastic lithosphere, we need to know the lithosphere's rheological properties. Assuming that the mineralogy of the mantle on Venus is essentially the same as on Earth, we can use experimental measurements of creep behavior for olivine aggregates (see, e.g., Karato et al. 1986; Hirth and Kohlstedt 1995) to constrain mantle viscosities for Venus. The major distinction between the conditions likely to prevail in the interior of Venus versus those of Earth is that continued volcanic activity on Venus in the presence of high surface temperatures has probably resulted in significant devolatilization of the crust and upper mantle on that planet (Kaula 1990,1995), whereas subduction beneath the oceans on Earth provides a return path for water into the interior. Thus, as the mechanical behavior of most silicate rocks is known to be affected by the presence of water, dry rheologies are likely to be the most appropriate for application to Venus.

Although detailed experimental studies have been performed on the mechanical behavior of upper mantle minerals and rocks (see, e.g., Kohlstedt et al. 1995), there have been few studies on crustal rocks with compositions similar to basalts. From measurements made on the composition of rocks for various parts of the surface of Venus by the Venera landers (Surkov et al. 1983,1984,1986), we infer that much of the surface of Venus is composed of basalts. The radar images of the surface of Venus by Magellan also indicate that there has been abundant large-scale deformation of the lithosphere, although there are few features that argue for plate tectonics as observed on Earth (see, e.g., Solomon et al. 1992; Phillips and Hansen 1994; Kaula 1995). Questions about the ability of the crust to dynamically support the topography, despite the high surface temperatures, and about the coupling of mantle dynamics to crustal deformation, require an assessment of the strength of the materials that comprise the crust on Venus. As noted above, we also wish to use the elastic thickness estimates of the previous two sections to assess lithospheric mechanical thickness and corresponding temperature gradient in various regions of Venus. This also requires a knowledge of crustal strength.

B. Previous Experimental Studies

There have been two published studies on the experimental rheologies of rocks of basaltic composition at conditions where plastic behavior will be dominant (Shelton and Tullis 1981; Caristan 1982). Both studies were performed on samples of a diabase (a rock of basaltic composition) from near Frederick, Maryland, that were either untreated or heated only on a hot plate prior to deformation. As this diabase contains several percent of hydrous minerals that do not dehydrate until temperatures above 500°C, it is believed that the hydrous minerals dehydrated during the deformation experiments, resulting in water-weakening of the minerals in the rock. Thus, these previous studies measured the mechanical behavior of diabase under undried conditions, which are not appropriate to the dry conditions expected in the crust on Venus.

C. Recent Experiments: Dry Diabase Measurements

Mackwell and his colleagues (Mackwell et al. 1995,1996) have performed creep experiments on dry diabase samples from near Frederick, Maryland (referred to as "Maryland diabase") and Columbia, South Carolina (referred to as "Columbia diabase"). Mineralogical properties of the samples and experimental procedures are described in the two references. Oxygen fugacity was controlled by using a Fe/FeO or Ni/NiO buffer.

The results of several of the deformation experiments on Columbia and Maryland diabase are illustrated in Figs. 5a,b. When the creep rate was measured at multiple temperatures or stresses in a single experiment, the initial temperature or stress was revisited later to test for irreversible changes in the sample during the deformation (such as grain growth, microfracturing, or partial melting). Given the sample-to-sample variability in modal composition and homogeneity, the reproducibility in creep rate between different samples of the same material deformed at the same conditions was remarkably good.

When all of the stress-strain rate data at a fixed temperature for each sample were fit using a linear least squares regression, values for the stress exponent n were determined. From these measurements, a value of $n = 4.8\pm0.6$ was calculated for the Columbia diabase, and $n = 4.7\pm1.0$ for the Maryland diabase, indicative of dislocation-controlled creep. Given the similarity of the stress exponents for the two diabase rocks, the stress exponents from all experiments were averaged to get $n = 4.7\pm0.8$ for dry diabase deformation. The creep activation energy Q for each diabase in the experiments was determined when the creep behavior was measured at a range of temperatures: $Q = 510 \pm 30$ kJ mol^{-1} for both the Columbia and Maryland diabases. The temperature ranges for each diabase were limited due to partial melting, the high activation energies for creep, and the limited range of stresses and strain rates available. Subsequently, flow laws for each rock were obtained.

For Columbia diabase,

$$\dot{\epsilon} = 4000\sigma^{4.7} \exp(-510/RT)$$

for the Fe/FeO buffered case;

$$\dot{\epsilon} = 1550\sigma^{4.7} \exp(-510/RT)$$

for the Ni/NiO buffered case; and for Maryland diabase,

$$\dot{\epsilon} = 77\sigma^{4.7} \exp(-510/RT)$$

for the Fe/FeO buffered case;

$$\dot{\epsilon} = 49\sigma^{4.7} \exp(-510/RT)$$

for the Ni/NiO buffered case, where the stress is in MPa and the activation energy is in kJ mol^{-1}. These flow laws are shown as dotted lines in Figs. 5a,b.

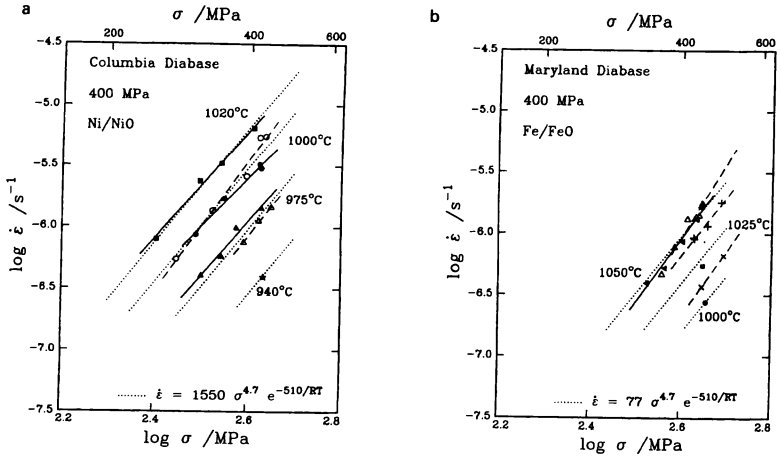

Figure 5. (a) Plot of strain rate versus stress for samples of Columbia diabase deformed at the Ni/NiO buffer at a confining pressure of 400 MPa. The solid symbols represent one experiment, the open symbols a second. The solid and dashed lines are linear least squares fits to the data at each temperature. Although the data from the two experiments at each temperature are in excellent agreement, two points at 1000°C appear to show higher strain rates than expected; we believe that these data probably include a component of microfracturing in the strain due to the high ratio of differential stress to confining pressure. The dotted lines represent the fit of the flow law at the bottom of the figure to the data. (b) Plot of strain rate versus stress for samples of Maryland diabase deformed at the Fe/FeO buffer at a confining pressure of 400 MPa. The solid symbols represent one experiment, the open symbols a second, and the + and × symbols a third; the results of the third experiment are somewhat stronger than the others, perhaps reflecting sample-to-sample variability in mineral composition. The solid and dashed lines are linear least squares fits to the data at each temperature. The dotted lines represent the fit of the flow law at the bottom of the figure to the data.

The ratio of the creep rates for the diabases from the two sources is about a factor of 30 to 50, with the Maryland diabase having the higher strength. By comparison, we observed little difference in the creep rate for the two diabase rocks resulting from the change in oxygen fugacity from Fe/FeO to Ni/NiO. The results of previous experimental studies of the deformation behavior of albite and anorthite (Shelton and Tullis 1981) and diopsidite (Kirby and Kronenberg 1984) bracket in strength the deformation behavior of the two diabases.

Optical microscope and scanning electron microscope investigations of the heat treated and deformed samples show little change in texture from the starting material. Transmission electron microscope investigations (J. C. White, personal communication) indicate that, while the bulk of the deformation in the Columbia diabase is localized within the plagioclase grains, the deformation in the Maryland diabase is distributed between the plagioclase and pyroxene grains. These observations are in general agreement with the observations of Kronenberg and Shelton (1980) on the undried Maryland diabase samples of Shelton and Tullis (1981) that show deformation predominantly in the plagioclase grains.

D. Comparison to Previous Flow Laws

The results of this study clearly illustrate the distinction between the strength of diabase under dry and wet conditions. Figure 6 is a lithospheric strength envelope (or yield strength envelope, YSE) plot of the strength of rock as a function of depth for a fixed strain rate of 10^{-15} s^{-1}; the relationship between temperature and depth is assumed to follow a simple linear form, and the surface temperature is taken as the mean surface temperature of Venus (470°C). At shallow depths (and low temperatures) the rock strength is defined by the brittle failure of the rock, which increases with increasing overburden pressure (depth); in this plot we use Byerlee's law (see, e.g., Goetze and Evans 1979; Brace and Kohlstedt 1980; Kohlstedt et al. 1995) to describe rock strength when the temperature is insufficient for plastic mechanisms to accommodate the stress. At a certain depth, depending on rock type, rates of deformation, and chemical environment, plastic processes within individual mineral grains become sufficiently active that the rock deforms predominantly by plastic mechanisms (the brittle-plastic transition). Below this depth, the rock strength follows the appropriate plastic flow law for the rock type appropriate for the depth range. In common geophysical application, the plastic flow law adopted is that of steady state creep.

In Fig. 6, the flow laws determined in this study for Columbia diabase and Maryland diabase (at the Fe/FeO buffer only) are plotted for representative Venus conditions, as well as flow laws for olivine aggregates (from Karato et al. 1986), and the previously published flow laws for Maryland diabase (MD, Caristan 1982; FD[ST], Shelton and Tullis 1981). As mentioned above, these latter studies on diabase were performed under conditions where the samples were wet, in that pretreatments only removed superficial water but

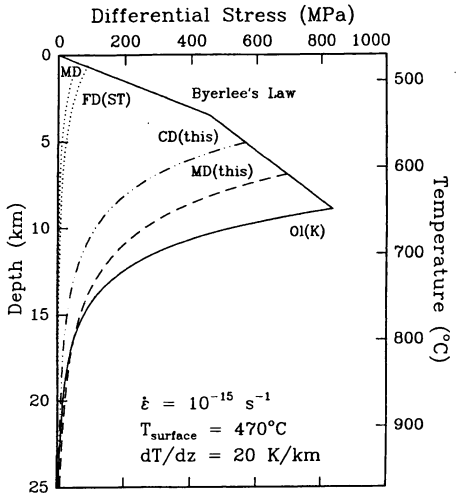

Figure 6. YSE plot of differential stress (essentially rock strength) vs depth for typical Venus conditions from the results of this study, (CD[this] and MD[this]), as well as the previous results on diabase from Shelton and Tullis (1981) (FD[ST]) and Caristan (1982) (MD), and olivine polycrystals from Karato et al. (1986) Ol(K). The relationship between rock strength and depth at shallow depths is assumed to follow Byerlee's law for frictional sliding (Kohlstedt et al. 1995).

not water trapped in hydrous minerals that dehydrated under run conditions. Thus, the new data for diabase deformation under dry conditions show it to be significantly stronger than the previous results, predicting much greater crustal strength and a deeper brittle-plastic transition.

E. Applications to Venus Rheology

Several general observations may be made based on application of these flow laws to Venus using relatively simple boundary conditions. One issue regards the existence of a strong-upper-crust/weak-lower crust/strong-upper-mantle lithospheric rheology (an "SWS" rheology, otherwise known as a "jelly-sandwich"). Uniform horizontal tension or compression applied to a rheologically stratified lithosphere leads, by instability growth, to creation of one or more dominant wavelengths of deformation depending on the stratification structure (Zuber 1987; see also Zuber and Parmentier 1990). Rift zones and ridge belts on Venus often have two dominant wavelength of deformation, indicative of an SWS rheology. The strong crust indicated by these new measurements of the ductile behavior of diabase provides an opportunity and a challenge to produce lithospheric rheology models that satisfy both the observational *and* experimental constraints (Zuber 1994). Section VI presents several hypotheses on how tectonic deformation exhibiting dominant wavelengths could exist in the face of a strong crustal rheology. Figure 7

shows YSEs for what might be considered "weak" and "strong" rheologies, having linear temperature gradients, strain rates, surface temperatures, and compositions (with fugacities) of 10 and 5 K km^{-1}, 10^{-17} and 10^{-15} s^{-1}, 470 and 447°C, and Columbia diabase (Fe/FeO) and Maryland diabase (Ni/NiO), respectively. Also shown are YSEs for weak and strong mantles using the olivine aggregate results of Karato et al. (1986). An apparent SWS rheology results from a 15-km-thick crust under weak conditions, whereas the crust shows no ductile behavior at all under strong conditions. On the other hand, a weak rheology with a 35-km-thick crust leads to both a weak lower crust and a weak upper mantle, and a strong rheology leads to a mild SWS. Finite deformation studies (see, e.g., Zuber and Parmentier 1996) in conjunction with these flow laws should provide important constraints on lithospheric structure.

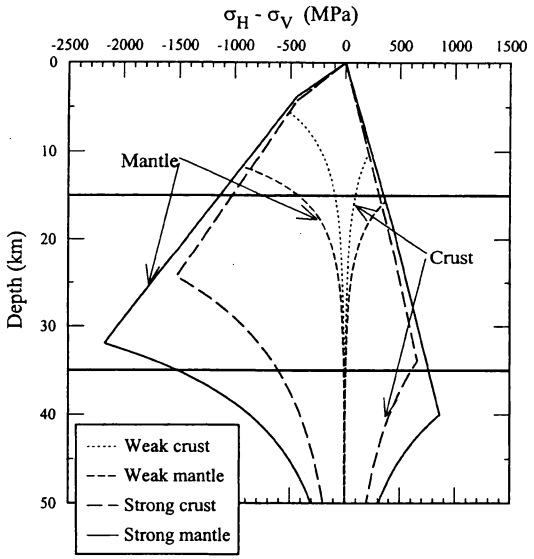

Figure 7. YSE plots for diabase (this work) and olivine aggregates under weak (short-dash for crust, medium-dash for mantle) and strong (long-dash for crust, solid for mantle) conditions. Weak: $dT/dz = 10$ K km^{-1}, $\dot{\epsilon} = 10^{-17}$ s^{-1}, surface temperature = 470°C, Columbia diabase (Fe/FeO buffer). Strong: $dT/dz = 5$ K km^{-1}, $\dot{\epsilon} = 10^{-15}$ s^{-1}, surface temperature = 447°C, Maryland diabase (Ni/NiO buffer). Horizontal lines mark crustal thicknesses discussed in text.

As the integrated area behind these strength versus depth plots is a measure of the lithospheric strength, we can make a number of general comments about predicted tectonic patterns on Venus. Although it is somewhat surprising given the high surface temperatures on Venus, the overall lithospheric strength is very high, and may be sufficiently high to permit isostatic (as well as flexural) support of topography over extended periods of geologic time. This observation may be sufficient to provide an explanation for the high correlation between gravity and topography in some regions, and limited relaxation of the impact craters. Another notable feature of these plots is that the contrast in strength of the rocks at the crust-mantle interface can be quite low under some conditions (Fig. 7). Such low contrast in rock strength permits strong dynamic coupling between the crust and mantle. Coupled with the probable lack of an asthenosphere or low viscosity channel on Venus (due to the absence of water in the Venusian uppermost mantle, and the large water-weakening effect in olivine, but also a reasonable inference from the deep apparent depths of isostatic compensation [Phillips 1986]), there may be a strong shear coupling of the convective motion in the interior of Venus to the upper portions of the lithosphere (Phillips 1986,1990). In the absence of the plate tectonic processes that occur on Earth, such coupling may explain the abundant tectonism and mountain building observed on Venus.

V. INELASTIC FLEXURE

A. Methodologies

With this review of lithospheric rheology, we can now reinterpret elastic thickness estimates presented in previous sections in terms of properties of the Venusian mechanical lithosphere. The elastic assumption inherent in the modeling in Secs. II and III is that bending moment $M(x)$ is linearly related, through the flexural rigidity D, to the curvature $C(x)$ of an elastic plate representing the lithosphere:

$$M(x) = -DC(x) \equiv -D\frac{d^2w(x)}{dx^2} \tag{2}$$

where $D = Eh^3/[12(1-\nu^2]$ (and E = Young's modulus, ν = Poisson's ratio, and h = plate thickness). It follows that the bending, or fiber, stress in the plate is linear but unbounded in z. But we have argued in the previous section that stress in the lithosphere is limited by a YSE. Only when stresses are less than the yield value can they be supported elastically (the "elastic core"); otherwise, they do not exceed the yield stress. That is, the YSE describes a lithosphere that is *elastic, perfectly plastic* and the flexure is *inelastic*. It follows that a nonlinear moment-curvature relationship results (Fig. 8). As the curvature increases in magnitude, the slope of the stress vs depth in the elastic core approaches zero and no further increase in moment is possible. This is known as *moment saturation* or a *plastic hinge*. Figure 8 serves to illustrate that the elastic thickness estimates obtained by geophysical methods are mathematical constructs that may act as surrogates for more realistic lithospheric rheologies.

In purely elastic problems, Eq. (2) is substituted into Eq. (1) to yield a fourth-order differential equation in $w(x)$, which is subject to analytic solution. In the elastic–plastic case this relationship is decidedly nonlinear and numerical methods must be employed for solution (Phillips 1990; Mueller

and Phillips 1995; Brown and Grimm 1996). The bending moment at any horizontal position on a thin plate is independent of rheology and is given, in the absence of in-plane forces, by (McNutt 1984)

$$M(x) = \int_x^\infty \Delta\rho g_0 w(x')(x' - x)\mathrm{d}x' \tag{3}$$

and must be balanced by the bending moment found by integrating the stress moment within the plate, which therefore is also independent of rheology. Thus, for any specific position on a deformed plate, corresponding to a specific curvature $C(x)$, elastic–plastic moment, $M_{EP}(x)$, and elastic moment must be equivalent (McNutt 1984)

$$M_{EP}[C(x), T(z), \Re] = \frac{ET_e^3}{12(1-\nu^2)}C(x) \tag{4}$$

where $T(z)$ is the temperature profile (often parameterized into a simple temperature gradient $\mathrm{d}T/\mathrm{d}z$) and $\Re$ is the collection of additional parameters needed to specify the YSE. If the appropriate curvature is specified, then the moments of the elastic thicknesses reviewed in Secs. II and III may be converted to their equivalent elastic–plastic moments and a temperature gradient can be estimated. Implicit in this approach is that the lithosphere deforms geometrically the same way for both the elastic and elastic–plastic rheologies (i.e., the curvatures match everywhere), but this is not always true.

Mueller and Phillips (1995) examined the conditions, on both Earth and Venus, under which a specific choice of curvature could accurately recover the mechanical thickness of the lithosphere, thus allowing reliable estimates of temperature gradient. Methods based on determining curvature from actual topographic profiles would seem to degenerate as the bending moment exceeds half of its saturation value. A method based on using the maximum curvature of the best fitting elastic profile to the observed topography seemed to do well up to at least 90% of moment saturation. However, small amounts of topographic noise can lead to large uncertainties in elastic thickness estimates and corresponding curvatures. In general, the moment-matching method can be expected to break down as saturation is approached (Brown and Grimm 1996).

B. Saturation Moments

Given the rheological models described in Sec. IV and estimates of saturation bending moment on Venus, one can estimate the temperature gradient within the mechanical portion of the lithosphere. Schubert and Sandwell (1995) categorized arcuate trenches to assess the possibility and significance of subduction on Venus. These arcuate features were chosen, in part, because they displayed downward flexures with curvatures exceeding about 2×10^{-7} m^{-1}. As shown in Fig. 8, such high curvatures indicate the plate is flexed beyond its elastic limit and is approaching a state of moment saturation, as discussed

above. Saturation bending moments were estimated at 15 sites using the methods described in Sec. II. While these areas were mostly poor candidates for estimating elastic and mechanical thickness because of their high outer rise curvatures and high topographic noise, they are adequate candidates for estimating saturation moments. In all 15 areas, between 4 and 14 altimeter profiles were modeled using the standard elastic methods. While elastic thickness estimates for these areas are unreliable on an individual profile basis, the moment estimates at the first zero crossing outboard of the trench will accurately reflect the moment due to the outer rise topography (Geotze and Evans 1979). (Table I "best" values [JS, SS] are based on the value of elastic thickness that gives the minimum RMS misfit to *all* profiles.) The flexure model simply provides a smooth curve for integrating the topography times the moment arm (Eq. 3); any smooth curve will serve the same purpose.

These estimates of saturation moment can be equated to the maximum moment that a lithosphere of prescribed rheology, strain rate, and temperature gradient can sustain. These results are given in Table III for a dry olivine rheology (Karato et al. 1986), a surface temperature of 717 K, and strain rates of 10^{-16} and 10^{-17} s^{-1}. Insofar as the estimated moments are not in complete saturation, then temperature gradients estimated will be upper bounds. Low thermal gradients of 4.8 to 4.1 K km^{-1} are needed to maintain the large observed moment at Artemis Corona. Brown and Grimm (1996) find much higher bending moment magnitudes along the eastern margin of Artemis ($\sim 70 \times 10^{16}$N), which require even lower thermal gradients (an upper bound of 4 K km^{-1}). This results, in part, because of the large in-plane force required to match the topographic profiles when inelastic flexural modeling is used (see Sec. V.D). Most of the other large flexures suggest temperature gradients of 6 to 10 K km^{-1} while the smaller features indicate higher temperature gradients (10–30 K km^{-1}). The flexures displaying small moments and thus high thermal gradients may reflect flexure of the upper crust or a decoupling between the crust and the mantle due to the presence of a jelly sandwich rheology. In these cases, our estimates of the temperature gradient may be much too high.

C. Moment-Matching Results

When good estimates of elastic thickness obtained from topographic profile matching are available, then direct moment matching (Eq. 4) is possible. Solomon and Head (1990) were the first to apply the McNutt (1984) moment-matching technique to Venus. They inverted an elastic thickness estimate based on a flexural interpretation of the topographic profile of the Freyja Montes foredeep. For an elastic thickness range of 11 to 18 km, they obtained a temperature gradient range of 23 to 14 K km^{-1}, using a strain rate of 10^{-16} s^{-1} and curvatures in the range of (1 to 2) $\times 10^{-7}$ m^{-1}. The corresponding mechanical thickness range is about 13 to 20 km.

Johnson and Sandwell (1994; see Sandwell and Schubert 1992*a*) also converted elastic thickness estimates (Sec. II) to mechanical thickness estimates

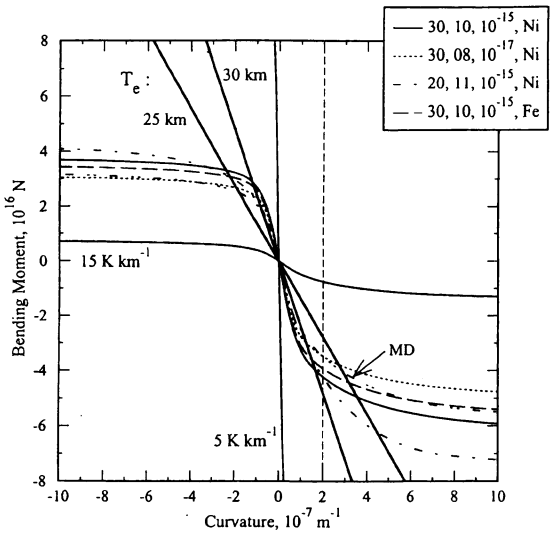

Figure 8. Bending moment vs curvature for 25- and 30-km-thick elastic plates and for elastic-perfectly plastic lithospheres whose stresses are limited by a YSE. Surface temperature is 720 K. The entries in the legend refer to crustal thickness, temperature gradient, strain rate, and oxygen fugacity conditions (see Sec. IV). The mantle has a dry olivine rheology (Goetze 1978). All curves are for Columbia diabase, except the curve labeled "MD," which is Maryland diabase. This curve has the same parameters as the bottom entry in the legend (≡ REF), except for a temperature gradient of 11 K km^{-1}. Using REF and invoking the dry olivine aggregate of Karato et al. (1986) produces a curve (not shown) that lies very nearly on the MD curve. Also shown are results with the same parameters as REF, except that temperature gradients are 5 and 15 K km^{-1}. Other parameter variations changed the curves very little. This included changing the surface temperature to 743 K (470°C) and changing the temperature profile from a linear to an error function form (Zuber and Parmentier 1990). The effective elastic lithosphere can be interpreted in terms of an elastic-plastic lithosphere where the two curves match for a specific curvature, in this case taken to be 2×10^{-7} m^{-1}.

h_m using Eq. (4) and the moment of the best fitting elastic profile at the point of maximum curvature and at the first zero crossing (Fig. 9). Temperature gradients are easily derived from mechanical thickness estimates in this work because the base of the mechanical lithosphere corresponds approximately to the 1030 K isotherm (inferred from Fig. 4 in Solomon and Head 1990) and the temperature gradient is constant. This yields $dT/dz \approx 290/h_m$, where h_m is in km and dT/dz is in K km^{-1}. Of the features modeled in Johnson and Sandwell (1994), five were considered sufficiently reliable to convert elastic thickness to mechanical thickness. These yielded for h_m a range of 21 to 37 km, and a corresponding temperature gradient range of 14 to 8 K km^{-1}.

Figure 8 invokes the moment-matching method to assess the temperature gradient beneath Atla Regio. The objective is to vary lithospheric rheology

TABLE III[a]

Saturation Moments and Maximum Temperature Gradients for Selected Features

Feature Name	Location		Moment	Curvature	dT/dz (K km^{-1}) $\dot{\epsilon}$ =	
	lat (°)	lon (°)	10^{16}N	10^{-7}m^{-1}	10^{-16}s^{-1}	10^{-17}s^{-1}
Neyterkob Corona	48.5	205.0	0.8	5.9	19.7	17.6
Nightingale Corona	61.0	131.0	0.7	1.6	20.6	18.5
S. Demeter Corona	53.0	298.0	2.0	3.2	13.6	11.9
N. Demeter Corona	57.0	294.0	3.1	4.6	11.3	9.9
W. Dali Chasma	−20.0	160.0	12.9	5.7	6.4	5.6
Artemis	−41.5	138.0	25.4	10.3	4.8	4.1
S. Latona Corona	−23.5	172.0	6.4	3.1	8.5	7.5
N. Latona Corona	−20.0	171.0	4.7	34.5	9.5	8.4
Eithinoha Corona	−57.3	8.2	1.0	3.3	18.1	16.1
Derceto Plateau	−47.6	19.7	0.2	209.4	27.2	25.6
E. Diana Chasma	−15.6	157.2	12.4	19.9	6.5	5.7
Hecate Chasma	16.5	248.4	2.4	3.7	12.6	11.0
Parga Chasma	−15.4	245.4	1.6	17.2	15.0	13.2
Uorsar Rupes	77.8	331.2	0.28	33.2	26.1	24.0
Quetzalpetlatl Corona	−66.6	350.0	0.85	9.8	19.2	17.2

[a] Table after Schubert and Sandwell (1995). Estimates of temperature gradient based on dry olivine rheology (Karato et al. 1986) and surface temperature of 717 K. dT/dz = temperature gradient; $\dot{\epsilon}$ = strain rate.

parameters to find the range of solutions that will match the moment range of 25- to 30-km-thick elastic lithospheres at the estimated maximum curvature of 2×10^{-7} m^{-1} (Phillips 1994). Crustal thickness, temperature gradient, strain rate, diabase composition, and oxygen fugacity were varied. It can be seen that matching the elastic moment is determined almost entirely by the temperature gradient; other parameters play a secondary role within reasonable ranges of plausibility. Acceptable solutions are within the range 8 to 11 K km^{-1}, and temperature gradients of 5 and 15 K km^{-1} are easily excluded. Results are given for strain rates of 10^{-15} and 10^{-17} s^{-1}. We note that the Johnson and Sandwell (1994) results are based on a strain rate of 10^{-16} s^{-1}. Grimm (1994) has used the degree of faulting of impact craters to infer that the near-surface strain rate on Venus has an upper bound of 10^{-17} s^{-1} over the span of time represented by the crater population. This strain rate gives the lowest temperature gradient, 8 K km^{-1}.

D. Inelastic Flexure Solutions

The actual deformation and stress state of an elastic–plastic rheology can be found by solving numerically the flexure equation (Eq. 1) with the nonlinear moment curvature relationship. Phillips (1990) obtained inelastic flexure solutions for model Venus lithospheres. He used the gravity field to estimate

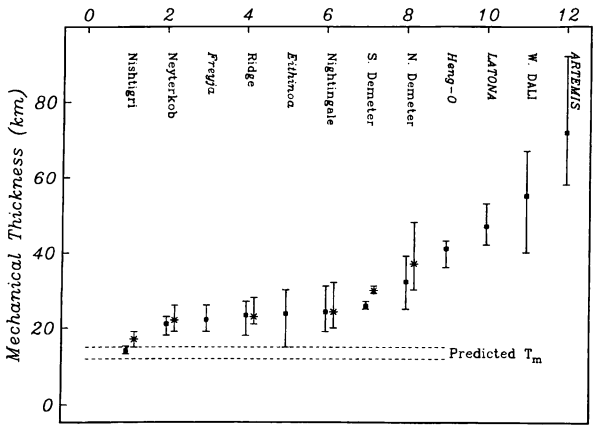

Figure 9. Mechanical thickness estimates derived from elastic thickness solutions for two-dimensional Cartesian flexure solutions of Johnson and Sandwell (1994), and from Sandwell and Schubert (1992*a*; italics in figure). See also Table I. Capitalized names are features that do not yield reliable estimates because they are thought to be moment saturated. Dashed lines indicate mechanical thickness based on Earth-scaled heat flow (Solomon and Head 1982). Square symbols and error bars are based on bending moment and curvature of first zero crossing of best fitting elastic profile (McNutt 1984); the asterisks and error bars correspond to the point of maximum curvature of the best-fitting elastic profile (Mueller and Phillips 1995) (figure from Johnson and Sandwell 1994).

in-plane force magnitudes under the assumption that the long wavelength gravity field is directly related to mantle convection that couples both shear and normal forces into the lithosphere. Solutions to the inelastic flexure equation were obtained for Venusian conditions using the dry websterite flow law of Avé Lallemant (1978). In response to the same surface load, deflection and bending moment of the lithosphere were significantly different under elastic rheology, elastic–plastic rheology, and elastic-plastic rheology with an estimated in-plane force of 3×10^{12} N m^{-1}.

Brown and Grimm (1996) carried out a detailed analysis of inelastic flexure at southeastern Artemis Chasma. Figure 10 is an "interaction diagram" showing inelastic solution properties as a function of applied bending moment and in-plane force. The solutions are bounded by a curve representing moment saturation as a function of the in-plane force. Contours to the right of this boundary are for the width of the outer rise at half of the maximum amplitude (FWHM). Also indicated in the figure is the domain of model solutions that satisfy the observed ranges of FWHMs and outer rise maximum amplitudes.

Given the large bending moment estimates, it is curious that normal faulting is not observed on the slope of the outer trench (chasma side of the outer rise) of southeast Artemis Chasma. If a compressional in-plane force is applied first, then application of a moment will cause unbending to

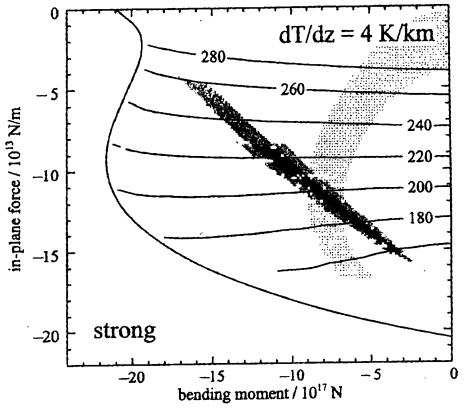

Figure 10. Interaction diagram for inelastic flexure of elastic–plastic plate with temperature gradient of 4 K km^{-1}. Axes are applied bending moment and applied in-plane load. Sinuous curve is the saturation bending moment resulting from the in-plane force. Contours are the outer rise width (km) at half of the maximum rise amplitude (FWHM). Diagonal shading indicates agreement (to within two standard deviations) with the observed FWHMs and outer rise maximum amplitudes at southeastern Artemis Chasma. The stippled region indicates those conditions for which no deformational failure (e.g, faulting) occurs at the surface, assuming that the surface has a finite strength of 50 MPa. A "strong" rheology was assumed to maximize temperature gradient (figure from Brown and Grimm 1996).

occur, leading to tensional failure at the surface. If, on the other hand, the in-plane force and bending moment are applied simultaneously, then Brown and Grimm (1996) propose that unloading can be neglected, leading to some solutions with surface stresses less than the assumed surface cohesion of 50 MPa. In this case, the interpretation is that the in-plane force does not arise from an external source (e.g., convective coupling; Phillips 1990), but from congestion at the trench itself. The stippled region in Fig. 10 indicates the solutions that have no surface faulting, and thus the intersection of this region with the acceptable FWHM/outer rise amplitude region indicates acceptable solutions overall. Brown and Grimm have devised a strong rheology model so as to maximize the temperature gradient (see their paper for details) and a temperature gradient of <4 K km^{-1} satisfies all three constraints over the spread of outer rise widths observed at southeast Artemis Chasma. A similarly low temperature gradient is obtained by the moment-matching technique (Sandwell and Schubert 1992*a*), but the elastic modeling results are insensitive to the magnitude of the in-plane force.

The in-plane force required for the Artemis inelastic model solutions, in the range -2 to -20×10^{13} N m^{-1} for the mean outer rise width, is large but similar to values inferred from modeling deformation in the central Indian Ocean lithosphere (McAdoo and Sandwell 1985; Karner and Weissel

1990). Trench congestion caused by regional impedance to subduction (the Indian-Asian collision impeding subduction of the Indo-Australian plate) can create forces this large. But the ultimate force driving the Indo-Australian plate is the subduction along a portion of its boundary. Mature subduction zones appear to be the only places where forces in excess of 10^{13} N m^{-1} in magnitude can be generated (Mueller and Phillips 1991), and in this case they appear to be transmitted across the plate, leading to intraplate deformation (see Cloetingh and Wortel 1986). Given the lack of water in the Venusian lithosphere and the low temperature gradients inferred at Artemis, in-plane forces in the upper end of the solution range are probably required to promote motion on throughgoing lithospheric faults in this region. Where such forces arise within the lithosphere and convecting mantle is a major question. The origin of the large bending moments required is also problematical.

We note that both the moment-matching and full inelastic flexural results have assumed that the crust and mantle are mechanically coupled. If they are not, due to a SWS rheology (see Sec. IV), then the bending moment decreases because the sum of separate crust and mantle bending moments is always less than the bending moment of the lithosphere taken as a single entity (see Burov and Diament 1995). A temperature gradient estimated from a coupled model will be an overestimate if the crust and mantle in the real lithosphere are, in fact, decoupled. Finally, if a lithospheric plate is progressively cooling, it will develop large thermal stresses. At regions of negative plate curvature, such as a trench, thermal stresses will increase the bending moment that can be supported. A plate will appear stronger (lower temperature gradient estimated) than it actually is if this effect is neglected (Wessel 1992). This mechanism, which can also delay normal faulting on the surface outboard of a trench, could be an important factor on Venus.

VI. TECTONICS AND STRENGTH STRATIFICATION

A. Introduction

Many areas of the Venus surface exhibit spatially extensive deformation features of both extensional and compressional origin that have been interpreted as rifts and mountain belts (Masursky et al. 1980; Campbell et al. 1983, 1984; Solomon and Head 1990; Solomon et al. 1992). The most prominent example of extensional deformation is Beta Regio, a rift zone associated with a major volcanic rise (Masursky et al. 1980; Campbell et al. 1984; Stofan et al. 1989; Senske et al. 1991). Fold and thrust structures are most commonly found in Ishtar Terra, particularly surrounding the Lakshmi Planum Plateau, though some have also been identified in the western part of Aphrodite Terra (Campbell et al. 1983; Kaula et al. 1992; Solomon et al. 1992; Suppe and Conners 1992; Keep and Hansen 1994; Williams et al. 1994). Extensional and compressional lineations are also observed over broad regions of the Venusian plains (Solomon et al. 1992; Squyres et al. 1992). Spatially extensive areas of more complex, and probably multiphase, deformation, termed tessera (or

complex ridged terrain), represent an additional deformation type that does not have a direct terrestrial analog.

B. Determination of Lithospheric Structure

Analyses based on Pioneer Venus (Masursky et al. 1980) and Venera 15 and 16 (Basilevsky et al. 1986) radar imaging revealed that a number of prominent structural assemblages exhibited generally regular feature spacings or widths, usually in the range 10 to 20 km. The spacings have been interpreted as dominant wavelengths of folding or stretching of lithospheric layers (see, e.g., Solomon and Head 1984). When structural deformation occurs at a characteristic wavelength, the wavelength can be used to constrain the thickness of the lithospheric layer. Before Magellan, application of flexural elastic (Solomon and Head 1984; Banerdt and Golombek 1988) and viscous and plastic instability (Zuber 1987) models yielded an elastic thickness or depth to the brittle–plastic transition for Venus generally in the range of 1 to 6 km, which is much less than comparable values observed for Earth. This range of values was viewed to be consistent with the idea that Venus ought to have a much thinner lithosphere than Earth owing to its much higher surface temperature (~700 K).

The recognition that many areas of Venus that display the short tectonic length scales also exhibit longer length scales of deformation (100–300 km) led to the suggestion that at least parts of the lithosphere may have a strong-weak-strong or jelly sandwich strength structure corresponding to a strong upper crust, weak lower crust and strong upper mantle (Zuber 1987; Banerdt and Golombek 1988). The multiple wavelengths led to constraints on crustal thickness (~10–30 km) and thermal gradient ($dT/dz < 25$ K km^{-1}) (Zuber 1987; Banerdt and Golombek 1988; Zuber and Parmentier 1990) that were in agreement with independent estimates derived from viscous relaxation models constrained by crater depths (Grimm and Solomon 1988). However, both the dominant wavelength and viscous relaxation models were based on rheological data for diabase crustal material that was, as discussed earlier, not fully dried (Shelton and Tullis 1981; Caristan 1982). Experimental results for dry diabase (Mackwell et al. 1995,1996), discussed in Sec. IV, indicate that a weak, lower crustal channel may in fact not be present on Venus, or may be sufficiently narrow that the upper and lower crust are not decoupled (see Sec. IV.E). The rheological results combined with the evidence from Magellan gravity and topography for a relatively thick elastic lithosphere on Venus (Johnson and Sandwell 1994; Moore et al. 1992; Sandwell and Schubert 1992*a*,*b*; Schubert et al. 1994; Phillips 1994; Smrekar 1994; Secs. II and III) may be in conflict with the idea of a very shallow brittle–plastic transition.

A conundrum thus arises as to how to explain the regions of deformation with small length scale tectonic fabrics. Magellan images have revealed that these features contain even finer-scale structure than previously recognized. The styles of deformation in many areas appear to be indicative of a lithosphere that is deforming as a plastic or viscous material without a significantly strong

elastic core. In fact, most models for fine scale compressional tectonics have invoked stacking or thrusting of layers, perhaps above a viscous or plastic detachment (Smrekar and Phillips 1988; Head 1990; Vorder Bruegge and Fletcher 1990; Suppe and Conners 1992; Williams et al. 1994). One possible explanation for this paradox is that much of the small-scale deformation dates from a time when the Venus lithosphere was much younger and hotter than present. If this is the case, it will ultimately be necessary to explain how the lithosphere thickness changed over time. Another possibility is that small-scale structure is controlled by intra-crustal layering, for example, by many superposed near surface volcanic flows. A third hypothesis is that mechanisms such as strain weakening (Zuber 1994) or velocity weakening (Neumann and Zuber 1995) could cause regional weakening of the lithosphere in areas of concentrated deformation. Yet another possibility is that the deformation is not controlled by a layer of a given thickness, but perhaps by subsurface shear. This has been suggested for lineations in some Venusian plains (Banerdt and Sammis 1992). It should be noted that all of these possibilities assume that the deformation indeed contains characteristic wavelengths. Magellan data have shown most areas to have more complex structures than previously appreciated, and length scales should be re-analyzed in a global sense.

While the small-scale aspect of the deformation is likely indicative of shallow structure, the broad spatial patterns of deformation provide evidence that compressional and extensional stresses that produced the deformation are a consequence of mantle dynamics (Phillips and Hansen 1994). Reconciling the spatial and temporal characteristics of extensional and compressional deformational structures into a self-consistent model for the thermal evolution is the major challenge in future study of these structures.

VII. SYNTHESIS

A. Introduction

Estimates of the effective elastic thickness remain, in the absence of seismic information and the direct measurements of heat flow, perhaps the only way geophysically in which to infer lithospheric thermal structure, providing such estimates can be converted to mechanical thicknesses. In this concluding section, we use such information to construct thermal models of the lithosphere. To proceed, we first review temperature gradients and heat fluxes inferred from elastic thickness estimates for various regions of the planet, and then come full circle to questions posed at the start of this chapter, comparing these results to convection models.

B. Inferences from Hotspot Results

1. Estimates of Temperature Gradient and Heat Flux. What do the hotspots tell us about temperature gradients on Venus, and how does this information relate to the heat flow at terrestrial hotspots? If, for consistency, we use just the results from the $\ell = 90$ gravity solution (chapter by Sjogren et al.), then elastic

thickness estimates at three hotspots (Atla, Bell, Western Eistla Regiones) range from 15 to 25 km. This range includes only the short wavelength results in the chapter by Smrekar et al. (see Table II here). Using a reference lithosphere ("REF", see Fig. 8) and the moment matching technique, linear temperature gradient is well fit by a relationship

$$dT/dz = 9.54\left(\frac{T_e}{30}\right)^{-0.817} \quad (5)$$

over a range of T_e from 10 to 40 km. The interval 15 to 25 km corresponds to a range in dT/dz of 17 K km^{-1} to 11 K km^{-1}. This temperature gradient must include the "mean" or background temperature gradient plus the contribution of the hotspot. Hotspot plumes probably come from the core-mantle boundary (see, e.g., Sleep 1990) and in a sense are superimposed on the dominant internally heated convection of the mantle. It is this latter phenomenon we wish to constrain.

The surface heat flux $\hat{q}$ corresponding to a given temperature gradient depends on the thermal conductivity K, which will have a significant radiative component in the Venusian lithosphere, given the high surface temperature. Because the temperature gradients estimated are in effect average values through the lithospheric column, we also use average thermal conductivities. Using expressions by Schatz and Simmons (1972), the average values of K for temperature gradients of 11 and 17 K km^{-1} are 3.3 and 3.8 W m^{-1} K^{-1}, respectively. This leads to a $\hat{q}$ range of 36 to 65 mW m^{-2} for these three hotspot regions.

2. Estimating the Plume Background or "Mean" Heat Flow. The estimated hotspot range can be used to infer a number more representative of the mean global heat flux only if the excess heat flow of the hotspot over that of the surrounding "ambient" mantle can be estimated. On Earth, this has been a difficult prospect. The excess heat flow at Hawaii, the "type" hotspot, may be at most 10 mW m^{-2} and is arguably consistent with zero (Von Herzen et al. 1989).

But models for the entrainment of hot plume material beneath the lithosphere (see, e.g., Sleep 1994) are intimately involved with the competition between the time scales of plate motion and diffusive thinning of the lithosphere. On Venus, with its presumably stationary lithosphere, heat delivered by plumes to the base of the lithosphere must eventually thin this region and elevate the surface heat flow unless heated portions of the lower lithosphere can be entrained in return flow to the deeper mantle. On Earth, excess heat flow associated with hotspots on slow moving plates appears to be in the range 10 to 20 mW m^{-2} (see, e.g., Sleep 1990; Phillips 1994) and this may be the closest analog to Venus. That is, the terrestrial lithosphere may be close to thermal equilibrium for these features and thus comparable to the zero-plate-velocity Venus.

On the other hand, model calculations by Smrekar and Parmentier (1996) show that the buoyancy flux (thermally anomalous mass per second delivered

by a plume) that produces topographic swells typical of Venusian hotspots is small by terrestrial standards. Typical model values are ~0.1 Mg s^{-1}. On the slow-moving Atlantic plate, the buoyancy fluxes estimated at the Cape Verde and Bermuda hotspots are 1.6 Mg s^{-1} and 1.1 Mg s^{-1}, respectively (Sleep 1990). The corresponding estimates of plume heat flux are 20 mW m^{-2} (Courtney and White 1986) and 11 mW m^{-2} (Detrick et al. 1986). Because the heat delivered by a plume is directly proportional to its buoyancy flux, these model results suggest that the excess heat flux delivered by Venusian mantle plumes may not be large.

Considering both types of arguments (terrestrial analogy, models), a reasonable estimate for the excess heat flux of Venusian plumes is 0 to 10 mW m^{-2}. The background, or "mean," heat flux would then lie between 36 and 55 mW m^{-2} if we link the two ranges (i.e., the upper end of the excess heat flux range is matched to the upper end of the Venusian range).

3. Comparison to Convection Modeling. This range of hotspot background or "mean" heat flux can be compared to estimates from parameterized convection models, from fully convective plume models matched to hotspot gravity/geoid and topography, and from Earth-scaled heat flow (Table IV).

TABLE IV
Estimates of Surface Heat Flux $\hat{q}$

Source (model or feature type)	$\hat{q}$, mW m^{-2}
Hotspots	
Atla, Bell, W. Eistla Regiones (see Table II)	36–65
"Background" from hotspots ≈ global mean	**36–55**[a]
Parameterized Convection Solutions (Global Mean)	
Non-stagnant lid (Phillips and Malin 1983 & updated)	**~50**
Stagnant lid (Solomatov and Moresi 1996)	**~15**
Phillips and Malin (1983) updated (stagnant lid, core cooling, modulated diffusion control of lithosphere)	**~35**
Earth-scaled Global Mean	
Solomon and Head (1982)	**74**
Turcotte (1995)	**63**
Artemis Chasma (Brown and Grimm 1996)	<12
Coronae, chasmata (see Table I)	45–100

[a] Numbers in bold are assessments of present-day "mean" heat flow on Venus.

A parameterized convection thermal model with no core heat component and with a chondritic heat source abundance produces a $\hat{q}$ of ~50 mW m^{-2} with a Nusselt number–Rayleigh number power exponent of 1/3 (see Phillips and Malin 1983). A similar value for heat flux was obtained by Solomatov and Moresi (1996) in parameterized convection calculations for Venus under approximately constant viscosity conditions (no stagnant lid).

Solomatov and Moresi (1996) obtain present-day estimates of stagnant lid (≈ thermal boundary layer) thickness and $\hat{q}$ of ~230 km and ~15 mW m^{-2}, respectively, for a parameterized convection model in which a constant viscosity regime is switched to a stagnant lid regime 0.6 Gyr ago. After the switch, the heat flux and lithospheric thickening are controlled purely by diffusion cooling of the lithosphere. These results are consistent with an "average" Venus scaled from stagnant lid convection solutions (interior Rayleigh number Ra = 3×10^6 and vertical viscosity contrast $\Delta\eta = 10^6$) adjusted to match the geoid, gravity field, and topography at Beta Regio.

We have updated the code of Phillips and Malin (1983) by introducing core cooling, by equating the thermal lithosphere explicitly with the upper thermal boundary layer, and by allowing for stagnant lid convection to set in at a specified time in the thermal history run. When the stagnant lid regime sets in, the thermal boundary layer thickness is controlled by diffusion cooling (Solomatov and Moresi 1996), but in our case the lithospheric thickness is also modulated by convective heat flux from beneath. In a run with chondritic heat sources and a switch to the stagnant lid regime 2 Gyr ago, the present value of $\hat{q}$ is about 35 mW m^{-2}, and the thickness of the thermal lithosphere is 120 km. Further work is required to elucidate the range of solutions possible with this approach. We note that this code in a nonstagnant lid regime (and with the usual determination of boundary layer thickness from the reciprocal of the Nusselt number) produces a present-day $\hat{q}$ of 53 mW m^{-2}. Table IV compares the estimated "mean" heat flow to parameterized convection solutions, as well as to the Earth-scaled estimates of 74 mW m^{-2} (Solomon and Head 1982) and 63 mW m^{-2} (Turcotte 1995).

The matching of plume convection models to the gravity/geoid and topography of hotspots is another potential method for determining lithospheric properties (Kiefer and Hager 1991,1992; Solomatov and Moresi 1996; Moresi and Parsons 1995; Smrekar and Parmentier 1996). Models that depend on bottom heating to create both a plume *and* an upper thermal boundary layer may be unrealistic. We expect that the upper thermal boundary is maintained by internally heated convection; it is disturbed by plumes initiated from the lower thermal boundary layer, which is maintained by modest amounts of heat released by the core. Such bottom-heated models are able to produce a spectrum of lithospheric thicknesses and heat fluxes, with the relative contributions of the plume and the thinned lithosphere to the gravity and topography fields varying amongst the models. Thus such models do not help distinguish between thick and thin lithospheres. Smrekar and Parmentier (1996), however, came close in spirit to modeling plume behavior superimposed on internally heating convection by launching plumes into a prespecified thermal structure that mimicked this condition. They showed that models with Earth-like mantle, lithosphere, and plume parameters can fit the range of geoid-to-topography ratios (GTRs) found for all likely Venusian hotspots. As noted above, the corresponding plume excess heat flux is quite small.

4. Summary. Elastic thickness determinations at hotspots lead to a range of estimated background $\hat{q}$ values, which, if equated with global average $\hat{q}$, significantly exceed values predicted by geoid/topography scaled stagnant lid parametrized convection results. Nonstagnant lid parameterized convection solutions fall within this range, but simple Earth-scaled values fall above. The modulated stagnant lid parameterized convection solution produces an Earth-like lithospheric thickness (120 km), and a $\hat{q}$ at the low end of the estimated range. Thus our estimate of Venus average heat flow seems to lie between a somewhat sluggish convective style predicted for the terrestrial planets in the absence of plate tectonics and a more Earth-like behavior, but with Venus mantle convection operating with less thermal efficiency than its terrestrial counterpart. This may be due, in part, to differences between the two planets in the mass of lithosphere subducted, as on Earth mantle cooling is strongly influenced by the heating of subducted slabs. In addition, the absence of plate tectonics increases the tendency for stratified convection, which leads to a lower flux (chapter by Schubert et al.). Another piece of evidence for Earth-like behavior, or at least not a thick stagnant lid, is that pressure-release partial melting may require a thin lithosphere (or very high plume and mantle temperatures) (Smrekar and Parmentier 1996). Additionally, the very low stress in the upper parts of a thick stagnant lid would severely inhibit rifting, which is contrary to observation.

C. Inferences from Corona/Chasma Results

Artemis Chasma is the most thoroughly studied of the Corona/Chasma features in terms of inelastic flexural modeling. As reviewed above, the temperature gradient is estimated to be less than 4 K km^{-1} (Brown and Grimm 1996); this corresponds to a heat flow of <12 mW m^{-2}. This result is not necessarily at odds with the conclusions drawn above, and might be expected if the underthrusting observed at Artemis Chasma (Brown and Grimm 1995) is associated with cold mantle downwelling.

Topography on Venus about 1 km on either side of the planetary mean radius follows a linear relationship between elevation and the normalized square root of cumulative area (Morgan and Phillips 1983; Rosenblatt et al. 1994). This same relationship is true generally for Earth's ocean floor, and this is to be expected from the depth dependence on the square root of plate age (for ages $\lesssim$100 Myr) resulting from diffusion cooling of the lithosphere. A simple model for Venus, with its immobile lithosphere, is a stochastic one; random impingement of mantle plumes at the base of the lithosphere, locally resetting its thermal age, should lead to the same result. Regional differences in heat flow of tens of mW m^{-2} are easily realizable in this scenario. As a lithosphere ages thermally, its degree of negative buoyancy increases, and, all other factors being equal, it may be more likely to initiate subduction (but see Cloetingh et al. 1989; Mueller and Phillips 1991). The proposed nascent subduction at Artemis Chasma (Sandwell and Schubert 1992*a*,*b*; Brown and Grimm 1995) and the low temperature gradient may both be pointing to a lithosphere that is thermally old in this region.

Flexure at Dali Chasma and Latona Corona may be moment saturated (see Fig. 9) so temperature gradient estimates by the moment-matching techniques are probably unreliable (Johnson and Sandwell 1994), although saturation moments (Table III) provide more dependable upper bounds. The remainder of the coronae, chasmata (and one ridge) have a T_e range, with one exception, that falls in the interval 10 to 20 km (Table I), corresponding to a heat flow range of 45 to 100 mW m^{-2}. This corresponds to a range from approximately the nonstagnant parameterized convection results to a value about 20% in excess of Earth's mean heat flux. Can these generally higher heat flows be reconciled with conclusions above? One possibility is that these (mostly) corona features represent an earlier, hotter time in Venus' history, but this seems unlikely given the relatively young average age of these features (Namiki and Solomon 1994; Price and Suppe 1994). A second possibility is that the flexure results are consistent with the heightened thermal environment of the proposed magmatic origin of most coronae (chapter by Stofan et al.). A third possibility is, of course, that the corona results are more representative of Venus and that Earth-scaled heat flux is the best model for Venus.

D. Concluding Remarks

We have attempted to summarize what is understood early in 1996 about the mechanical and dynamic state of the lithosphere of Venus. Our emphasis has been on using properties of the lithosphere to constrain the thermal state of the planet, for this is one of the most fundamentally interesting goals of lithospheric studies on planets where seismic and direct heat flow information are not available.

Further progress can be expected from (i) combined modeling of lithospheric flexure and mantle convection, (ii) an improved understanding of regional age differences, (iii) improvements in gravity field representations—higher spherical harmonic degree expansions and improved local modeling, (iv) new dynamical models of the lithosphere to explain multiple scales of deformation, and (v) continuing experiments on rock deformation under Venusian conditions.

Acknowledgments. S. Smrekar and R. Grimm provided useful, constructive reviews of this chapter. M. Zimmerman and D. Kohlstedt worked with SJM in performing the deformation experiments on diabase, and J. White is currently working with SJM analyzing the deformation microstructures in the experimentally deformed samples. Many of us were supported by NASA grants.

REFERENCES

Avé Lallemant, H. G. 1978. Experimental deformation of diopside and websterite. *Tectonophysics* 48:1–27.

Banerdt, W. B., and Golombek, M. P. 1988. Deformational models of rifting and folding on Venus. *J. Geophys. Res.* 93:4759–4772.

Banerdt, W. B., and Sammis, C. G. 1992. Small-scale fracture patterns on the volcanic plains of Venus. *J. Geophys. Res.* 97:16149–16166.

Basilevsky, A. T., et al. 1986. Styles of tectonic deformations on Venus: Analysis of Veneras 15 and 16 data. *J. Geophys. Res.* 91:D399–D412.

Bechtel, T. D., Forsyth, D. W., and Swain, C. J. 1987. Mechanisms of isostatic compensation in the vicinity of the East African Rift, Kenya. *Geophys. J. Roy. Astron. Soc.* 90:445–465.

Brace W. F., and Kohlstedt D. L. 1980. Limits on lithospheric stress imposed by laboratory experiments. *J. Geophys. Res.* 85:6248–6252.

Brown, C. D., and Grimm, R. E. 1995. Tectonics of Artemis Chasma: A Venusian "plate" boundary. *Icarus* 117:219–249.

Brown, C. D., and Grimm, R. E. 1996. Lithospheric rheology and flexure at Artemis Chasma, Venus. *J. Geophys. Res.* 101:12697–12708.

Burov, E. B., and Diament, M. 1995. The effective elastic thickness (T_e) of continental lithosphere: What does it really mean? *J. Geophys. Res.* 100:3905–3927.

Byerlee, J. D. 1978. Friction of rocks. *Pageoph.* 116:615–626.

Campbell, D. B., Head, J. W., Harmon J. K., and Hine, A. A. 1983. Venus: Identification of banded terrain in the mountains of Ishtar Terra. *Science* 221:644–647.

Campbell, D. B., Head, J. W., Harmon J. K., and Hine, A. A. 1984. Venus: Volcanism and rift formation in Beta Regio. *Science* 226:167–170.

Caristan, Y. 1982. The transition from high temperature creep to fracture in Maryland diabase. *J. Geophys. Res.* 87:6781–6790.

Cloetingh, S., and Wortel, R. 1986. Stress in the Indo-Australian plate. *Tectonophysics* 132:49–67.

Cloetingh, S., Wortel, R., and Vlaar, N. J. 1989. On the initiation of subduction zones. *Pageoph.* 129:7–25.

Courtney, R. C., and White, R. S. 1986. Anomalous heat flow and geoid across the Cape Verde Rise: Evidence for dynamic support from a thermal plume in the mantle. *Geophys. J. Roy. Astron. Soc.* 87:815–868.

DeBremaecker, J. C. 1977. Is the oceanic lithosphere elastic or viscous? *J. Geophys. Res.* 82:2001–2004.

Detrick, R. S., et al. 1986. Heat flow observations on the Bermuda Rise and thermal models of mid-plate swells. *J. Geophys. Res.* 91:3701–3723.

Dorman, L. M., and Lewis, B. T. R. 1970. Experimental isostasy 1. Theory of the determination of the Earth's isostatic response to a concentrated load. *J. Geophys. Res.* 70:3357–3365.

Ebinger, C. J., Bechtel, T. D., Forsyth, D. W., and Bowin, C. O. 1989. Effective elastic plate thickness beneath the East African and Afar Plateaus and dynamic compensation of the uplifts. *J. Geophys. Res.* 94:2883–2901.

Evans, S. A., Simons, M., and Solomon, S. C. 1992. Flexural analysis of uplifted rift flanks on Venus. In *International Colloquium on Venus*, LPI Contrib. No. 789, pp. 30–32 (abstract).

Ford, P. G., and Pettengill, G. H. 1992. Venus topography and kilometer-scale slopes. *J. Geophys. Res.* 97:13103–13114.

Forsyth, D. W. 1985. Subsurface loading and estimates of the flexural rigidity of continental lithosphere. *J. Geophys. Res.* 90:12623–12632.

Goetze, C. 1978. The mechanisms of creep in olivine. *Phil. Trans. Roy. Soc. London A* 288:99–119.

Goetze, C., and Evans, B. 1979. Stress and temperature in the bending lithosphere as constrained by experimental rock mechanics. *Geophys. J. Roy. Astron. Soc.* 59:463–478.

Grimm, R. E. 1994. Recent deformation rates on Venus. *J. Geophys. Res.* 99:23163–23171.

Grimm, R. E., and Solomon, S. C. 1988. Viscous relaxation of impact crater relief on Venus: Constraints on crustal thickness and thermal gradient. *J. Geophys. Res.* 93:11911–11929.

Head, J. W. 1990. Formation of mountain belts on Venus: Evidence for large-scale convergence, underthrusting, and crustal imbrication in Freyja Montes, Ishtar Terra. *Geology* 18:99–102.

Hirth, G., and Kohlstedt, D. L. 1995. Experimental constraints on the dynamics of the partially molten upper mantle: 2. Deformation in the dislocation creep regime. *J. Geophys. Res.* 100:15441–15449.

Janes, D. M., and Squyres, S. W. 1995. Viscous relaxation of topographic highs on Venus to produce coronae. *J. Geophys. Res.* 100:21137–21187.

Janes, D. M., et al. 1992. Geophysical models for the formation and evolution of coronae on Venus. *J. Geophys. Res.* 97:16055–16067.

Johnson, C., and Sandwell, D. T. 1994. Lithospheric flexure on Venus. *Geophys. J. Intl.* 119:627–647.

Karato, S., Paterson, M. S., and FitzGerald, J. D. 1986. Rheology of synthetic olivine aggregates: Influence of grain size and water. *J. Geophys. Res.* 91:8151–8176.

Karner, G. D., and Weissel, J. K. 1990. Factors controlling the location of compressional deformation of oceanic lithosphere in the central Indian Ocean. *J. Geophys. Res.* 95:19795–19810.

Kaula, W. M. 1990. Venus: A contrast in evolution to Earth. *Science* 247:1191–1196.

Kaula, W. M. 1995. Venus reconsidered. *Science* 270:1460–1464.

Kaula, W. M., et al. 1992. Styles of deformation in Ishtar Terra and their implications. *J. Geophys. Res.* 97:16085–16120.

Keep, M., and Hansen, V. L. 1994. Structural history of Maxwell Montes, Venus: Implications for Venusian mountain belt formation. *J. Geophys. Res.* 99:26015–26028.

Kiefer, W. S. 1995. Mantle plumes with temperature-dependent rheology and implications for the origin of volcanic rises on Venus. *Eos: Trans. AGU Suppl.* 76(46):F342 (abstract).

Kiefer, W. S., and Hager, B. H. 1991. A mantle plume model for the equatorial highlands of Venus. *J. Geophys. Res.* 96:20947–20966.

Kiefer, W. S., and Hager, B. H. 1992. Geoid anomalies and dynamic topography from convection in cylindrical geometry: Applications to mantle plumes on Earth and Venus. *Geophys. J. Intl.* 108:198–214.

Kirby, S. H., and Kronenberg, A. K. 1984. Deformation of clinopyroxenite: Evidence for a transition in flow mechanisms and semibrittle behavior. *J. Geophys. Res.* 89:3177–3192.

Kohlstedt, D. L., Evans B., and Mackwell, S. J. 1995. Strength of the lithosphere: Constraints imposed by laboratory experiments. *J. Geophys. Res.* 100:17587–17602.

Konopliv, A. S., and Sjogren, W. L. 1994. Venus spherical harmonic gravity model to degree and order 60. *Icarus* 112:42–54.

Kronenberg, A. K., and Shelton, G. L. 1980. Deformation microstructures in experimentally deformed Maryland diabase. *J. Struct. Geology* 2:341–353.

Lewis, B. T. R., and Dorman, L. M. 1970. Experimental isostasy 2. An isostatic

model for the U.S.A. derived from gravity and topography data *J. Geophys. Res.* 70:3367–3386.

Mackwell, S. J., Zimmerman, M. E., Kohlstedt, D. L., and Scherber, D. S. 1995. Experimental deformation of dry Columbia diabase: Implications for tectonics on Venus. In *Rock Mechanics: Proc. 35th U. S. Symposium*, eds. J. J. K. Daeman and R. A. Shultz (Brookfield, Vt.: A. A. Balkema), pp. 207–214.

Mackwell, S. J., Bystricky, M., White, J. C., Zimmerman, M. E., and Kohlstedt, D. L. 1996. High temperature deformation of dry diabase, with application to crustal deformation on Venus. *Lunar Planet. Sci. Conf.* XXVII:793–794 (abstract).

Masursky, H., et al. 1980. Pioneer Venus radar results: Geology from images and altimetry. *J. Geophys. Res.* 85:8232–8260.

McAdoo, D. C., and Sandwell, D. T. 1985. Folding of oceanic lithosphere. *J. Geophys. Res.* 90:8563–8569.

McKenzie D., and Bowin, C. 1976. The relationship between gravity and bathymetry in the Atlantic Ocean. *J. Geophys. Res.* 81:1903–1915.

McKenzie D., and Nimmo, F. 1996. Elastic thickness estimates for Venus from line of sight accelerations. *Icarus*, submitted.

McKenzie, D., et al. 1992. Features on Venus generated by plate boundary processes, *J. Geophys. Res.* 97:13533–13544.

McNutt, M. K. 1984. Lithospheric flexure and thermal anomalies. *J. Geophys. Res.* 89:11180–11194.

McNutt, M. K. 1988. Thermal and mechanical properties of the Cape Verde Rise. *J. Geophys. Res.* 93:2784–2794.

McNutt, M. K., and Shure, L. 1986. Estimating the compensation depth of the Hawaiian Swell with linear filters. *J. Geophys. Res.* 91:13915–13923.

Melosh, H. J. 1978. Dynamic support of outer rise topography. *Geophys. Res. Lett.* 5:321–324.

Moore, W., Schubert, G., and Sandwell, D. T. 1992. Flexural models of trench/outer rise topography of coronae on Venus with axisymmetric spherical shell thin elastic plates. In *International Colloquium on Venus*, LPI Contrib. No. 789, pp. 72–73 (abstract).

Moresi, L., and Parsons, B., 1995. Interpreting gravity, geoid, and topography for convection with temperature dependent viscosity: Application to surface features on Venus. *J. Geophys. Res.* 100:21155–21171.

Moresi, L. N., and Solomatov V. S. 1995. Numerical investigation of 2D convection with extremely large viscosity variations, *Phys. Fluids* 7:2154–2162.

Morgan, P., and Phillips, R. J. 1983. Hot spot heat transfer: Its application to Venus and implications to Venus and Earth. *J. Geophys. Res.* 88:8305–8317.

Mueller, S., and Phillips, R. J. 1991. On the initiation of subduction. *J. Geophys. Res.* 96:651–665.

Mueller, S., and Phillips, R. J. 1995. On the reliability of lithospheric constraints derived from models of outer-rise flexure. *Geophys. J. Intl.* 123:887–902.

Namiki, N., and Solomon, S. C. 1994. Impact crater densities on volcanoes and coronae on Venus: Implications for volcanic resurfacing. *Science* 265:929–933.

Neumann, G. A., and Zuber, M. T. 1995. A continuum approach to the development of normal faults. In *Rock Mechanics: Proc. 35th U. S. Symposium*, eds. J. J. K. Daeman and R. A. Shultz (Brookfield, Vt.: A. A. Balkema), pp. 191–198.

Phillips, R. J. 1986. A mechanism for tectonic deformation on Venus. *Geophys. Res. Lett.* 13:1141–1144.

Phillips, R. J. 1990. Convection-driven tectonics on Venus. *J. Geophys. Res.* 95:1301–1316.

Phillips, R. J. 1994. Estimating lithospheric properties at Atla Regio, Venus. *Icarus* 112:147–170.

Phillips, R. J., and Hansen, V. L. 1994. Tectonic and magmatic evolution of Venus. *Ann. Rev. Earth Planet. Sci.* 22:597–654.

Phillips, R. J., and Malin, M. C. 1983. The interior of Venus and tectonic implications. In *Venus*, eds. D. M. Hunten, L. Colin, T. M. Donahue and V. I. Moroz (Tucson: Univ. of Arizona Press), pp. 159–214.

Press, W. H., Teukolsky, S. A., Vetterling, W. T. and Flannery, B. P. 1992. *Numerical Recipes in FORTRAN* (Cambridge: Cambridge Univ. Press).

Price, M., and Suppe, J. 1994. Mean age of rifting and volcanism on Venus deduced from impact crater densities. *Nature* 372:756–759.

Rosenblatt, P., Pinet, P. C., and Thouvenot, E. 1994. Comparative hypsometric analysis of Earth and Venus. *Geophys. Res. Lett.* 21:465–468.

Sandwell, D. T., and Schubert, G. 1992*a*. Flexural ridges, trenches, and outer rises around coronae on Venus. *J. Geophys. Res.* 97:16069–16083.

Sandwell, D. T., and Schubert, G. 1992*b*. Evidence for retrograde lithospheric subduction on Venus. *Science* 257:766–770.

Saunders, R. S., et al. 1992. Magellan mission summary. *J. Geophys. Res.* 97:13067–13090.

Schatz, J. F., and Simmons, G. 1972. Thermal conductivities of Earth materials at high temperatures. *J. Geophys. Res.* 77:6966–6983.

Schubert, G., and Sandwell, D. T. 1995. A global survey of possible subduction sites on Venus. *Icarus* 117:173–196.

Schubert, G., Moore, W. B., and Sandwell, D. T. 1994. Gravity over coronae and chasmata on Venus. *Icarus* 112:130–146.

Senske, D. A., Head, J. W., Stofan, E. R., and Campbell, D. B. 1991. Geology and structure of Beta Regio, Venus: Results from Arecibo radar imaging. *Geophys. Res. Lett.* 18:1159–1162.

Shelton, G., and Tullis, J. 1981. Experimental flow laws for crustal rocks. *Eos: Trans. AGU* 62:396.

Simons, M. 1996. Localization of Gravity and Topography: Constraints on the Tectonics and Mantle Dynamics of Earth and Venus. Ph.D. Thesis, Massachusetts Inst. of Technology.

Sleep, N. H. 1990. Hotspots and mantle plumes: Some phenomenology. *J. Geophys. Res.* 95:6175–6736.

Sleep, N. H. 1994. Lithospheric thinning by midplate mantle plumes and the thermal history of hot plume material ponded at sublithospheric depths. *J. Geophys. Res.* 99:9327–9343.

Smrekar, S. E. 1994. Evidence for active hotspots on Venus from analysis of Magellan gravity data. *Icarus* 112:2–26.

Smrekar, S., and Parmentier, E. M. 1996. The interaction of mantle plumes with surface thermal and chemical boundary layers: Applications to hotspots on Venus. *J. Geophys. Res.* 101:5397–5410.

Smrekar, S., and Phillips, R. J. 1988. Gravity-driven deformation of the crust on Venus. *Geophys. Res. Lett.* 15:693–696.

Solomatov, V. S. 1993. Parameterization of temperature-and stress-dependent viscosity convection and the thermal evolution of Venus. In *Flow and Creep in the Solar System: Observations, Modeling and Theory*, eds. D. B. Stone and S. K. Runcorn (Dordrecht: Kluwer), pp. 131–145.

Solomatov, V. S. 1995. Scaling of temperature- and stress-dependent viscosity convection, *Phys. Fluids* 7:266–274.

Solomatov, V. S., and Moresi, L. N. 1996. Stagnant lid convection on Venus. *J. Geophys. Res.* 101:4737–4753.

Solomon S. C., and Head, J. W. 1982. Mechanisms for lithospheric heat transport on Venus: Implications for tectonic style and volcanism. *J. Geophys. Res.* 87:9236.

Solomon, S. C., and Head, J. W, 1984. Venus banded terrain: Tectonic models for band formation and their relationship to lithospheric thermal structure. *J. Geophys. Res.* 89:6885–6897.

Solomon, S. C., and Head, J. W. 1990. Lithospheric flexure beneath the Freyja Montes foredeep, Venus: Constraints on lithospheric thermal gradient and heat flow. *Geophys. Res. Lett.* 17:1393–1396.

Solomon, S. C., et al. 1992. Venus tectonics: An overview of Magellan observations. *J. Geophys. Res.* 97:13199–13255.

Squyres, S. W., et al. 1992. Plains tectonism on Venus: The deformation belts of Lavinia Planitia. *J. Geophys. Res.* 97:13579–13599.

Stofan, E. R., et al. 1989. Geology of a rift zone on Venus: Beta Regio and Devana Chasma. *Geol. Soc. Amer. Bull.* 101:143–156.

Suppe, J. and Conners, C. 1992. Critical-taper wedge mechanics of fold-and-thrust belts on Venus: Initial results from Magellan. *J. Geophys. Res.* 97:13545–13561.

Surkov, Yu. A., et al. 1984. New data on the composition, structure and properties of Venus rock obtained by Venera 13 and 14. *J. Geophys. Res.* 89:B393–B402.

Surkov, Yu. A., et al. 1983. Determination of the elemental composition of rocks on Venus by Venera 13 and 14. *J. Geophys. Res.* 88:A481–A493.

Surkov, Yu. A., et al. 1986. Venus rock composition at the Vega 2 landing site. *J. Geophys. Res.* 91:E215–E218.

Turcotte, D. L. 1995. How does Venus lose heat? *J. Geophys. Res.* 100:16931–16940.

Turcotte, D. L., and Schubert, G. 1982. *Geodynamics: Applications of Continuum Physics to Geological Problems* (New York: J. Wiley).

Von Herzen, R. P., Cordery, M. J., Detrick, R. S., and Fang, C. 1989. Heat flow and the thermal origin of hot spot swells: The Hawaiian Swell revisited. *J. Geophys. Res.* 94:13783–13799.

Vorder Bruegge, R. W., and Fletcher, R. C. 1990. A model for the shape of overthrust zones on Venus. *Lunar Planet. Sci. Conf.* XXI:1278–1279 (abstract).

Wessel, P. 1992. Thermal stresses and the bimodal distribution of elastic thickness estimates of the oceanic lithosphere. *J. Geophys. Res.* 97:14177–14193.

Williams, C. A., Conners, C., Dahlen, F. A., Price E. J., and Suppe, J. 1994. Effect of the brittle-ductile transition on the topography of compressive mountain belts on Earth and Venus. *J. Geophys. Res.* 99:19947–19974.

Zuber, M. T. 1987. Constraints on the lithospheric structure of Venus from mechanical models and tectonic surface features. *J. Geophys. Res.* 92:E541–E551.

Zuber, M. T. 1994. Rheology, tectonics and the structure of the Venus lithosphere. *Lunar Planet. Sci. Conf.* XXV:1575–1576 (abstract).

Zuber, M. T., and Parmentier, E. M. 1990. On the relationship between isostatic elevation and the wavelengths of tectonic surface features on Venus. *Icarus* 85:290–308.

Zuber, M. T., and Parmentier, E. M. 1996. Formation of fold-and-thrust belts on Venus by thick-skinned deformation. *Nature* 377:704–707.

Zuber, M. T., Bechtel, T. D., and Forsyth, D. W. 1989. Effective elastic thicknesses of the lithosphere and mechanisms of isostatic compensation in Australia. *J. Geophys. Res.* 94:9353–9367.

THE CRUST OF VENUS

ROBERT E. GRIMM
Arizona State University

and

PAUL C. HESS
Brown University

Surface geochemical measurements and the morphology of volcanic structures imaged from orbit indicate that the surface of Venus is dominated by basalt. Even unusual geochemical signatures and volcanic landforms suggestive of silicic lavas are consistent with mafic to intermediate bulk compositions. Gravity data indicate that the mean thickness of the crust is 20 to 50 km; 30 km is the value preferred here. The planet's smooth hypsometry and the dominance of deep isostatic compensation argue that the crust has a comparatively uniform thickness, departing significantly only in the tessera highlands. The crust at present occupies 1 to 2% of the total volume of Venus. By contrast, Earth's present fractional volume of basaltic crust is ~0.5%, but may integrate to ~10% over the last 4 Gyr due to crustal recycling. In spite of the recent evidence from the Magellan mission that Venus underwent strong volcanotectonic resurfacing at or before several hundred million years ago, it is still unknown whether such resurfacing included significant crustal recycling. Recycling is required if the bulk of the present crust was generated by horizontal accretion analogous to seafloor spreading. However, full development of horizontal crustal accretion is difficult to envision because of the depth and temperature of melting necessary to generate basaltic crust so much thicker than terrestrial oceanic crust. In addition, the bulk composition of the crust must be picritic to komatiitic and a late global flooding event must conceal features diagnostic of earlier lithospheric recycling. Alternatively, a dry, stiff upper mantle may have allowed only limited horizontal movements, and vertical accretion dominated crustal generation. A tholeiitic to picritic crust could be formed at numerous regional centers of lithospheric extension during episodes of global activity. During periods of global quiescence, alkali basalts would be a significant melt component produced by minor stretching of a thick lithosphere or plume melting beneath a rigid lid. Recycling of crust is possible but not necessary in this model. The present crust is probably too thin to be globally limited by densification and detachment due to the granulite/eclogite phase transitions, but such controls, especially locally, cannot be ruled out. Efficient distribution of magma or subsequent solid-state creep is necessary to inhibit large permanent lateral variations in crustal thickness under vertical accretion. Contemporary crustal production is 0.01 to 0.4 $km^3 yr^{-1}$, less than or equal to the intraplate crustal formation rate of Earth.